

FABRICATION AND TESTING OF A SENSITIVE ULTRAVIOLET-VISIBLE
SILICON PHOTODIODE DEVICE

by

José de la Luz Martínez Montes

A Dissertation Submitted to the Faculty of the
DEPARTMENT OF ELECTRICAL ENGINEERING
In Partial Fulfillment of the Requirements
For the Degree of
DOCTOR OF PHILOSOPHY
In the Graduate College
THE UNIVERSITY OF ARIZONA

1 9 7 9

INFORMATION TO USERS

This was produced from a copy of a document sent to us for microfilming. While the most advanced technological means to photograph and reproduce this document have been used, the quality is heavily dependent upon the quality of the material submitted.

The following explanation of techniques is provided to help you understand markings or notations which may appear on this reproduction.

- 1. The sign or "target" for pages apparently lacking from the document photographed is "Missing Page(s)". If it was possible to obtain the missing page(s) or section, they are spliced into the film along with adjacent pages. This may have necessitated cutting through an image and duplicating adjacent pages to assure you of complete continuity.**
- 2. When an image on the film is obliterated with a round black mark it is an indication that the film inspector noticed either blurred copy because of movement during exposure, or duplicate copy. Unless we meant to delete copyrighted materials that should not have been filmed, you will find a good image of the page in the adjacent frame.**
- 3. When a map, drawing or chart, etc., is part of the material being photographed the photographer has followed a definite method in "sectioning" the material. It is customary to begin filming at the upper left hand corner of a large sheet and to continue from left to right in equal sections with small overlaps. If necessary, sectioning is continued again—beginning below the first row and continuing on until complete.**
- 4. For any illustrations that cannot be reproduced satisfactorily by xerography, photographic prints can be purchased at additional cost and tipped into your xerographic copy. Requests can be made to our Dissertations Customer Services Department.**
- 5. Some pages in any document may have indistinct print. In all cases we have filmed the best available copy.**

**University
Microfilms
International**

300 N. ZEEB ROAD, ANN ARBOR, MI 48106
18 BEDFORD ROW, LONDON WC1R 4EJ, ENGLAND

7912537

MARTINEZ MONTES, JOSÉ DE LA LUZ
FABRICATION AND TESTING OF A SENSITIVE ULTRAVIOLET-
VISIBLE SILICON PHOTODIODE DEVICE.

THE UNIVERSITY OF ARIZONA, PH.D., 1979

University
Microfilms
International

300 N ZEEB ROAD, ANN ARBOR, MI 48106

FABRICATION AND TESTING OF A SENSITIVE ULTRAVIOLET-VISIBLE
SILICON PHOTODIODE DEVICE

by

José de la Luz Martínez Montes

A Dissertation Submitted to the Faculty of the
DEPARTMENT OF ELECTRICAL ENGINEERING
In Partial Fulfillment of the Requirements
For the Degree of
DOCTOR OF PHILOSOPHY
In the Graduate College
THE UNIVERSITY OF ARIZONA

1 9 7 9

THE UNIVERSITY OF ARIZONA
GRADUATE COLLEGE

I hereby recommend that this dissertation prepared under my direction
by José de la Luz Martínez Montes
entitled FABRICATION AND TESTING OF A SENSITIVE
ULTRAVIOLET-VISIBLE SILICON PHOTODIODE DEVICE
be accepted as fulfilling the dissertation requirement for the Degree
of DOCTOR OF PHILOSOPHY.

Reginald L. Call
Dissertation Director

2 January 1979
Date

As members of the Final Examination Committee, we certify that we have
read this dissertation and agree that it may be presented for final
defense.

Reginald L. Call

2 January 1979
Date

Roger C. Jones

2 January 1979
Date

Quinn

1/5/79
Date

Date

Date

Final approval and acceptance of this dissertation is contingent on the
candidate's adequate performance and defense thereof at the final oral
examination.

STATEMENT BY AUTHOR

This dissertation has been submitted in partial fulfillment of requirements for an advanced degree at The University of Arizona and is deposited in the University Library to be made available to borrowers under rules of the Library.

Brief quotations from this dissertation are allowable without special permission, provided that accurate acknowledgment of source is made. Requests for permission for extended quotation from or reproduction of this manuscript in whole or in part may be granted by the head of the major department or the Dean of the Graduate College when in his judgment the proposed use of the material is in the interests of scholarship. In all other instances, however, permission must be obtained from the author.

SIGNED:

Jose Martinez.

ACKNOWLEDGMENTS

Special thanks are given to Dr. R. L. Call, my major professor and advisor, who helped and encouraged me in the preparation of this dissertation. A very grateful acknowledgment is given to Dr. J. N. Fordemwalt, Director of the Solid State Laboratories of The University of Arizona, for allowing me to use the facilities. I also express my appreciation to Dr. R. C. Jones, Professor, who allowed me to use the Quantum Electronics Laboratory facilities.

It is a pleasure to acknowledge deeply to Estela Gómez for helping me in the study of the surface state charge generation experiments. Finally, my sincere thanks to people of México, who through CONACYT supported my education.

TABLE OF CONTENTS

	Page
LIST OF ILLUSTRATIONS	vi
LIST OF TABLES	viii
ABSTRACT	x
 CHAPTER	
1 INTRODUCTION	1
Mathematical Model for the SiO ₂ -Si Light Detector . . .	3
2 STUDY OF SURFACE STATE CHARGE	11
Experimental Assumptions	12
Experimental Procedure	17
Anodic Oxidation of Si	20
Metal Deposition	22
Measurement of C-V Curves	22
Materials Used	25
Results	25
Discussion of Results	35
Summary	42
3 THEORETICAL QUANTUM EFFICIENCY	44
A Simplified Model	44
Calculation of Parameters	45
Current Density Calculations	50
Discussion	56
Summary	59
4 FABRICATION OF THE ANODIC SiO ₂ -Si LIGHT DETECTOR	61
Geometrical Arrangement of the Device	61
Materials Used	63
Fabrication Procedures	63
Anodic Oxide Growth Assumptions	63
Ion Implantation of Phosphorus	64

TABLE OF CONTENTS (Continued)

	Page
Metallization Procedures	65
Measurement Procedures	65
Results	69
Discussion of Results	69
Summary	75
5 SUMMARY AND CONCLUSIONS	77
Summary	77
Recommendations for Future Work	79
APPENDIX A: PROCEDURE FOR Si WAFER CLEANING	80
APPENDIX B: PREPARATION OF MOLAR SOLUTIONS	81
APPENDIX C: SiO ₂ GROWTH CHARACTERISTICS OF WAFERS	82
APPENDIX D: RELATIVE INTENSITY LINES FOR A Hg LAMP	84
APPENDIX E: LISTING OF A NUMERICAL SOLUTION PROGRAM	85
APPENDIX F: ANODIC OXIDATION OF SILICON WAFERS	87
APPENDIX G: PHOSPHORUS ION IMPLANTATION PROCEDURE	88
APPENDIX H: ALUMINUM EVAPORATION PROCEDURE	89
APPENDIX I: PARAMETER CALCULATION FOR PHOSPHORUS ION IMPLANT .	90
LIST OF REFERENCES	92

LIST OF ILLUSTRATIONS

Figure		Page
1.1	Energy Diagram for an Anodic SiO ₂ -Si Light Detector under Dark Conditions	4
1.2	Electric Field E _s as Function of the Electrostatic Potential φ _s	7
2.1	Energy Diagrams for an MIS System	13
2.2	C-V Curve of an MIS System	16
2.3	C-V Curves under Different Conditions	18
2.4	Experimental Arrangement for Anodic Oxidation of Si . .	21
2.5	Geometrical Arrangement of an MIS Capacitor	23
2.6	Experimental Arrangement for the Measurement of the C-V Characteristics of Anodic SiO ₂ and MOS Capacitors . .	26
2.7	Typical Forming Voltage and SiO ₂ Thickness versus Growing Time Curves	37
2.8	Average Q _{SS} Generation versus Different Molarity Growth Conditions	39
2.9	Percentage in Change in Q _{SS} Generation versus Different Molarity Growth Conditions	41
3.1	(1-R) Coefficient versus Wave Length of an SiO ₂ -Si System	48
3.2	Calculated Electron Current Density Spectral Response for the SiO ₂ -Si Light Detector	51
3.3	Flow Diagram for a Fourth Ordered Runge-Kutta-Nystrom Numerical Analysis	54
3.4	Calculated Hole Current Density Spectral Response of an n ⁺ -diffused Junction Detector and a Field Induced Detector	55

LIST OF ILLUSTRATIONS (Continued)

Figure		Page
3.5	Total Current Density Spectral Response Comparison between an n/p Diffused and a Field Induced SiO ₂ -Si Light Detector	57
3.6	Calculated Quantum Efficiency of the SiO ₂ -Si Light Detector	58
4.1	Geometrical Arrangement of the Anodic SiO ₂ -Si Light Detector	62
4.2	Experimental Arrangement to Measure the Spectral Response of the SiO ₂ -Si Light Detector	67
4.3	Ideal Diode I-V Curve with Offset Voltage and a Series Resistance	68
4.4	Sensitivity Spectral Response of the Anodic SiO ₂ -Si Light Detector	70
4.5	Comparison between Theoretical and Experimental Quantum Efficiencies for the SiO ₂ -Si Light Detector	71
4.6	I-V Characteristics of the SiO ₂ -Si Light Detector under a Fluorescent Light Lamp	73

LIST OF TABLES

Table		Page
2.1	Anodic Silicon Dioxide Growth Conditions for Several Si Wafers	27
2.2	Density of Surface State Charge of Several MIS Capacitors	28
2.3	Anodic Silicon Dioxide Growth Conditions for the Second Batch of Si Wafers	28
2.4	Density of Surface State Charge of the Second Batch of MIS Capacitors	29
2.5	Anodic Silicon Dioxide Growth Conditions for the Third Batch of Silicon Wafers	30
2.6	Density of Surface State Charge of the MIS Capacitors .	30
2.7	Anodic Silicon Dioxide Growth Conditions for the 4th Batch of Silicon Wafers	31
2.8	Density Surface State Charge of the 4th Batch of MIS Capacitors	31
2.9	Anodic Silicon Dioxide Growth Conditions for the 5th Batch of Silicon Wafers	32
2.10	Density of Surface State Charge of the 5th Batch of MIS Capacitors	32
2.11	Anodic Silicon Dioxide Growth Conditions for the 6th Batch of Silicon Wafers	33
2.12	Density of Surface State Charge of the 6th Batch of MIS Capacitors	33
2.13	Anodic Silicon Dioxide Growth Conditions for the 7th Batch of Silicon Wafers	34
2.14	Density of Surface State Charge of the 7th Batch of MIS Capacitors	35

LIST OF TABLES (Continued)

Table		Page
2.15	Comparison between the Average Electric Field and the Average Surface Charge Generation with Different Oxide Growth Conditions	40
3.1	Wavelength Variation of the Indexes of Refraction of SiO ₂ and Si	47
3.2	Typical Parameters of a .10 ohm x m p-type Si Material	49
4.1	Anodic Oxide Growth Conditions for Batch I	64
4.2	Calculated Parameters for Phosphorus Ion Implantation in the SiO ₂ -Si Device	65
4.3	Results in the Calculations of R, and R _{s2}	72

ABSTRACT

This dissertation presents an investigation on the low temperature fabrication of a new ultraviolet-visible light detector. Interface charges between a low temperature grown anodic silicon dioxide and a silicon single crystal material are used to generate a strong electric field perpendicular to the photodetection surface of the device. This electric field separates the photon created electron-hole pairs in the silicon material to produce a net flux of electric current across the detector.

Experimental optimization studies for surface state charge generation in the anodic silicon dioxide-silicon interface are presented.

An approximate one dimensional numerical analysis is employed to calculate the theoretical quantum efficiency of the device. Comparisons between the theoretical and experimental quantum efficiencies are made.

Ion implantation and low temperature anodic oxide growth technologies are employed for the fabrication of the light detector device. These techniques allow fabrication of this type of light detector device at temperatures no greater than 620°C.

CHAPTER 1

INTRODUCTION

It has been known that light detection below the $0.4 \mu\text{m}$ range by semiconductor devices possesses problems. Wide band gap materials such as Gallium Phosphide (GaP), Cadmium Sulfide (CdS), Gallium Arsenide (GaAs), etc. have small minority carrier diffusion lengths (Tyagai 1964). This situation, causes some of the photon generated electron-hole pairs to be lost by recombination processes across the semiconductor material before they can be extracted from the detector device. On the other hand, narrow band gap materials such as Silicon (Si), Germanium (Ge), etc. have high absorption coefficients. This situation causes most of the photon generated electron-hole pairs to be produced close to the active surface of the material where they can be lost by recombination with the always present surface state traps.

Taking advantage of the long diffusion length of minority carriers in narrow band semiconductors it is possible to enhance the light detection of these detectors, in the range $0.4 \mu\text{m}$ or below, by using very shallow diffused p-n junctions in photodiode devices. The presence of an electric field generated by this shallow diffused p-n junction helps the electron-hole pairs to avoid loss by recombination processes with surface states traps (Lindmayer and Allison 1973). Shallow diffused p-n junctions however, decrease the lifetime of

minority carriers due to the strain in lattice deformation and interstitial lattice traps created by diffused impurity atoms in the crystal.

Solar cells as light detectors, with electric field induced shallow junctions, have been investigated by Call (1973). Cells of this type do not require impurity diffusion on the active area of the device. The electric field, across the Silicon Dioxide-Silicon (SiO_2 -Si) interface of this type of detector, is generated by positive sodium impurity atoms in the thermal SiO_2 layer. Call (1973), has also studied SiO_2 -Si cells with positive Q_{ss} charges produced at the SiO_2 -Si interface of thermal SiO_2 . These studies on electric field induced junction devices, however, require high temperature fabrication cycles. High temperature processing of single crystal silicon wafers reduces the lifetime minority carriers in these materials due to thermal lattice deformation. Thermal stress on single crystals are known to generate: defects, distortions, and faults in the crystal lattices. These type of irregularities act as traps or "lifetime killing centers" of minority carriers in semiconductor materials.

The low temperature growth techniques of anodic silicon dioxide offer the possibility of study the electric field induced junction light detector devices as an alternative to the high temperature ($> 650^\circ\text{C}$) fabrication of light detector devices. It is the purpose of this dissertation to study this possibility. The broad objectives of the dissertation are:

1. The experimental study of the interface charges of the anodic SiO_2 -Si.
2. Calculation of the theoretical quantum efficiency of the anodic SiO_2 -Si light detector.
3. Fabrication of an anodic SiO_2 -Si light detector.
4. Comparison between the theoretical and experimental quantum efficiency of the anodic SiO_2 -Si light detector.

Mathematical Model for the SiO_2 -Si Light Detector

Operation of the SiO_2 -Si light detector relies upon the presence of a strong electric field at the interface of an SiO_2 -Si system. This electrical field in the surface of the Si materials is strong enough to cause the intrinsic Fermi energy, of p-type material, to cross the equilibrium Fermi energy level and produce an n-type inversion layer at the surface of the Si crystal. Fig. 1.1 shows the thermal equilibrium energy diagram of an SiO_2 -Si interface light detector. Electron-hole pairs, generated by photons hitting the surface region of the Si material, are separated by the presence of this electric field. This charge separation is such that excess generated carriers create a net flux of charge current across the SiO_2 -Si device. The existing electric field at the SiO_2 -Si interface is generated by the presence of positive interface charges, in the SiO_2 -Si transition region, so its intensity depends upon the density of positive interface charges.

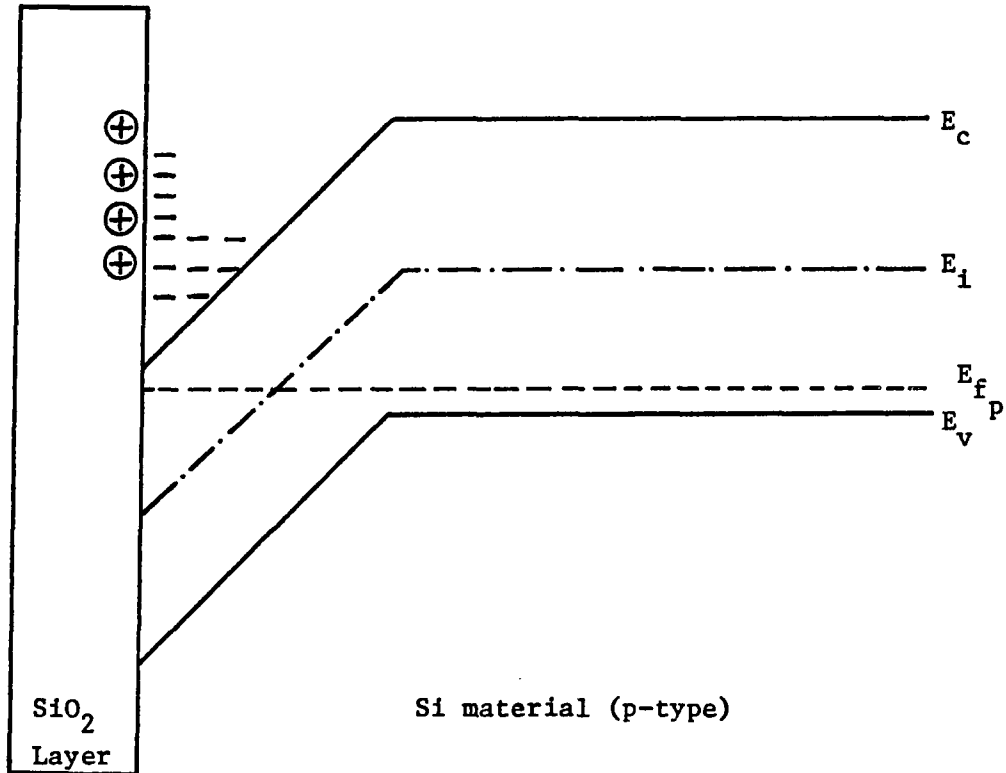


Fig. 1.1 Energy Diagram for an Anodic SiO_2 -Si Light Detector under Dark Conditions

E_c = Conduction Band Energy Level

E_v = Valence Band Energy Level

E_i = Intrinsic Energy Level

E_{fP} = Equilibrium Fermi Energy Level

⊕ = Surface State Charge Q_{ss}

— = Free electrons in the conduction band

An analysis of the $\text{SiO}_2\text{-Si}$ light detector quantum efficiency requires a knowledge of the electric field at the $\text{SiO}_2\text{-Si}$ interface and the electron and hole current density across the field induced p-n junction. The quantum efficiency of a non-amplifying light detector is the ratio

$$Q(\lambda) = \frac{n_E}{n_{ph}} = \frac{J(\lambda)hc}{\Phi_e(\lambda)q\lambda} \quad (1.1)$$

where

$J(\lambda)$ = total current density flowing across the non-amplifying detector.

h = Planck constant

c = light velocity in vacuum

λ = wavelength of incident radiation

$\Phi_e(\lambda)$ = incident radiant power density or radiant flux falling onto the light detector.

The above equation defines the ratio of a certain number of electrons, n_E , flowing into an external electric circuit per unit time to the number of photons, n_{ph} , falling on the photodetector per unit time (Chappell, 1976). Previous analysis of the electric field, generated by the presence of positive charges on the surface of a semiconductor material, was investigated by Brown (1953), and Kingston and Neustadter (1955). The electric field at the $\text{SiO}_2\text{-Si}$ interface is given as

$$E^2(\phi) = \left(\frac{2KT}{q} \right)^2 \left(\frac{qp_{po}B}{2e_s} \right) [(\exp(-B\phi) + B\phi - 1) + \frac{n_{po}}{p_{po}} (\exp(B\phi) - B\phi - 1)] \quad (1.2)$$

where

q = electron charge

p_{po} = equilibrium hole concentration

K = Boltzman constant

T = absolute temperature

e_s = semiconductor permittivity

$$B = \frac{q}{KT}$$

ϕ = electrostatic potential

n_{po} = equilibrium electron concentration

The value of the electric field, E_s , at the surface of the semiconductor is given by

$$E^2(\phi_s) = \left(\frac{2KT}{q} \right)^2 \left(\frac{qp_{po}B}{2e_s} \right) F\left(\phi_s, \frac{n_{po}}{p_{po}}\right) \quad (1.3)$$

where

$$F\left(\phi_s, \frac{n_{po}}{p_{po}}\right) = [(\exp(-B\phi) + B\phi_s - 1) + \frac{n_{po}}{p_{po}} (\exp(B\phi_s) - B\phi_s - 1)] \quad (1.4)$$

ϕ_s = value of the electrostatic potential at the surface of the semiconductor. Its value is influenced by the amount of positive charges present on the surface of the semiconductor. Fig. 1.2 shows

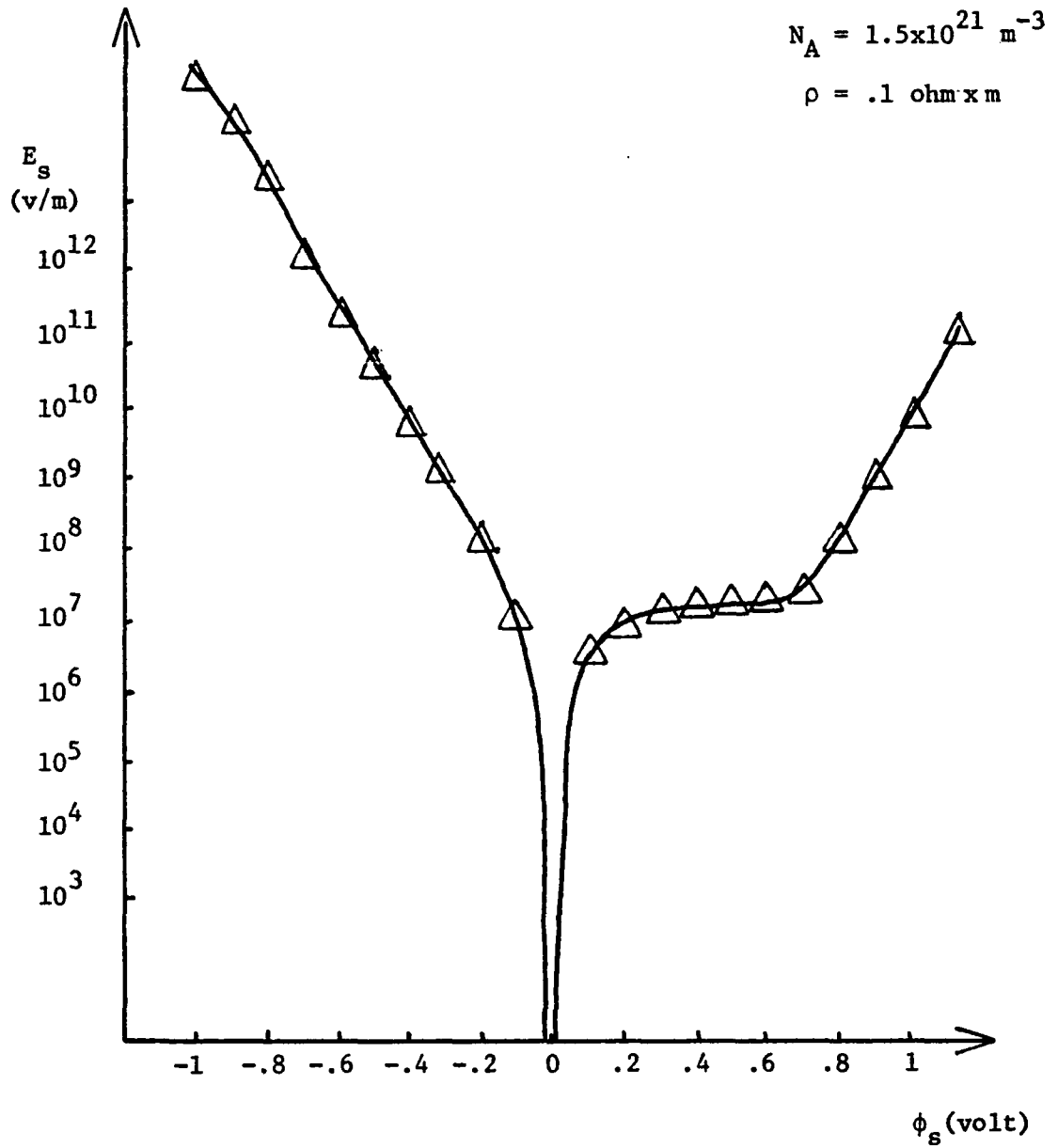


Fig. 1.2 Electric Field E_s as a Function of the Electrostatic Potential ϕ_s

$E_s = E_s(\phi_s)$ as a function of ϕ_s for a given semiconductor material. This shows three important regions. The accumulation region for which $\phi_s < 0$. This situation corresponds to negative charges on the surface of the semiconductor. The depletion and weak inversion region for which $0 < \phi_s < 2\phi_B$. This situation corresponds to low density of positive charges on the semiconductor. The strong inversion region for which $\phi_s > 2\phi_B$. This situation corresponds to a high density of positive charges on the surface of the semiconductor. The value of the field induced p-n junction, x_j , is calculated by integrating, from the surface value ϕ_s to the intrinsic value ϕ_i , the electrostatic potential equation

$$x_j = \int_{\phi_s}^{\phi_i} \frac{d\phi}{\frac{2KT}{qL_D} F\left(\phi, \frac{n_{po}}{p_{po}}\right)} \quad (1.5)$$

where

$$L_D = \text{Debye length} = \left(\frac{2KT^e_s}{p_{po}q} \right)^{1/2}$$

Calculations of the total current density are made by solving the approximated minority carrier current equations (one dimension).

For the p-type side

$$J_e \approx qD_n \frac{d\delta n}{dx} \quad (1.6)$$

For the inversion n-type side

$$J_p = -qD_p \frac{d\delta p}{dx} + q\mu_p \delta PE(x) \quad (1.7)$$

where

D_n = electron diffusion constant

δ_n = excess electron concentration

D_p = hole diffusion constant

δ_p = excess hole concentration

and the total current density through the device is given as

$$J_T = J_e + J_p \quad (1.8)$$

Eqns. (1.6) and (1.7) can be solved with help of the continuity equation for electron and holes

$$\frac{d^2 \delta_n}{dx^2} - \frac{1}{D_n \tau_n} \delta_n = - \frac{\phi_0 \exp(-\alpha x)}{D_n} [1 - R(\lambda)] \alpha \quad (1.9a)$$

$$\begin{aligned} \frac{d^2 \delta_p}{dx^2} - \frac{qE(x)}{KT} \frac{d\delta_p}{dx} - \left(\frac{1}{D_p \tau_p} + \frac{q}{KT} \frac{dE}{dx} \right) \delta_p \\ = - \frac{\phi_0 \exp(-\alpha x)}{D_p} [1 - R(\lambda)] \alpha \end{aligned} \quad (1.9b)$$

where

ϕ_0 = number of incident photons per unit time unit area

t_p = hole life time in n-side

t_n = electron life time in p-side

R = reflection coefficient of the SiO_2 -Si interface

α = absorption coefficient of Si

The boundary conditions for Eqns. (1.9a), (1.9b) are for the p-side

$$D_p \frac{d\delta p}{dx} = s_p \delta p \quad \text{at } x = 0 \quad (1.10a)$$

$$\delta p = 0 \quad \text{at } x = x_j \quad (1.10b)$$

Eq. (1.10a) states the presence of recombination centers, at the surface of the semiconductor, with recombination velocity s_p . Eq. (1.10b) states that the hole minority carriers are swept away by the electric field as soon as they cross the induced p-n junction at $x = x_j$. For the n-side

$$\delta n = 0 \quad \text{at } x = x_j \quad (1.11a)$$

$$\delta n = 0 \quad \text{at } x = H \quad (1.11b)$$

where

H = thickness of p-region. Eq. (1.11a) states that electron excess carriers are swept away by the electric field as soon as they cross the induced p-n junction at $x = x_j$. Eq. (1.11b) states the presence of an ohmic contact at $x = H$. Eq. (1.9a) is solved by standard solution methods. The spatial dependence of the electric field, due to positive density of charges at the SiO_2 -Si interface, requires that Eq. (1.9b) be solved only by approximate numerical methods.

CHAPTER 2

STUDY OF SURFACE STATE CHARGE

The interface charge states of the MIS system have not been advantageously utilized by solid state designers. The presence of small amounts of surface charge states and surface states in MIS devices have detrimental effects on the electrical properties of such structures. These interface charge and surface states can alter considerably the value of the electrostatic potential from the bulk to the surface of the semiconductor materials in MIS devices. Deviation of the bulk value of the electrostatic potential at the surface of a semiconductor can produce the enhancement, depletion or inversion of surface density of majority carriers and thus alter the electrical properties of the interface. Interface studies of MIS structures by Grove et al. (1965), showed the existence of a surface state charge of positive polarity in n-type and p-type thermal oxidized silicon materials. Deal et al. (1967), pointed out that this fixed positive surface state charge, Q_{ss} , is due to excess silicon species introduced in the oxide layer, near the SiO_2 -Si interface, during thermal oxidation of silicon. It is now known that the nature of the fixed surface state charge is due to an intermediate reaction product of the oxidation process of silicon (Raider and Berman 1978).

It is the objective of this part of the dissertation to study experimentally the electrical properties of the anodic low temperature grown SiO_2 -Si interface. The aim of this study is toward three important objectives:

1. To avoid destroying the minority carrier lifetime in the Si material.
2. To inhibit creation of fast surface traps at the SiO_2 -Si interface.
3. To create enough surface states charges, at the SiO_2 -Si interface, to invert the minority carriers in the Si surface.

Experimental Assumptions

The experimental method of study employed in this part of the work is by measuring the capacitance versus voltage characteristics of MIS structures. This method allows determination of interface charges, SiO_2 impurity contamination and presence of fast surface states in the Metal- SiO_2 -Si system.

The presence of an electric field, perpendicular to the surface of a semiconductor, is generated by the total number of charges, Q_s , per unit area in the semiconductor (Sze 1969), given by the relation

$$Q_s = - \frac{2e KT}{qL_D} F \left(B\phi_s, \frac{n_{po}}{p_{po}} \right) \quad (2.1)$$

Fig. 2.1 shows the energy diagrams of an MIS system for different values of the external applied voltage, V, where

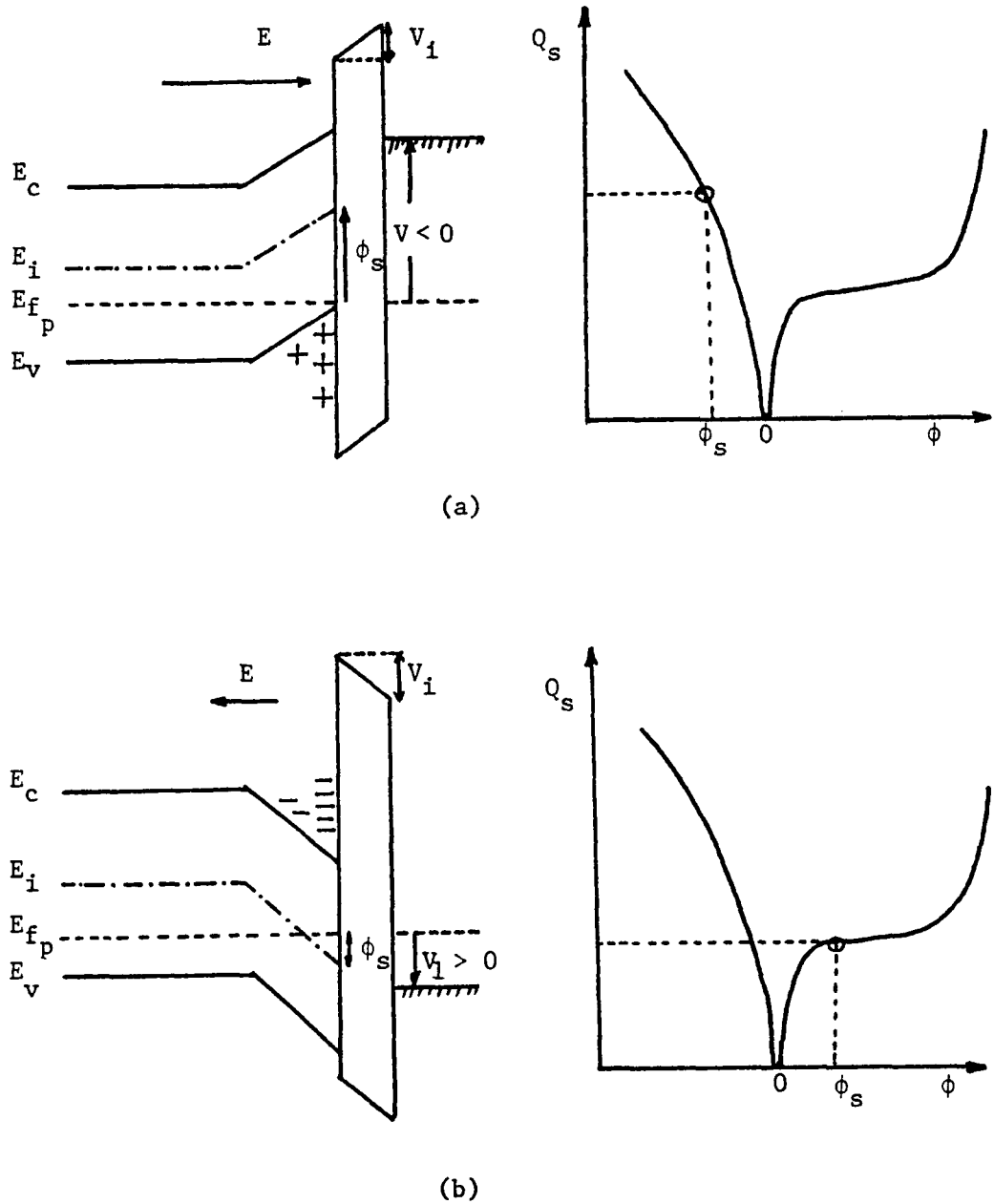


Fig. 2.1 Energy Diagrams for an MIS System

- (a) For an external applied voltage $V < 0$, there is an accumulation of positive charges at the SiO_2 -Si interface.
- (b) For an external applied voltage $V_1 > 0$, there is an accumulation of negative charges at the SiO_2 -Si interface.

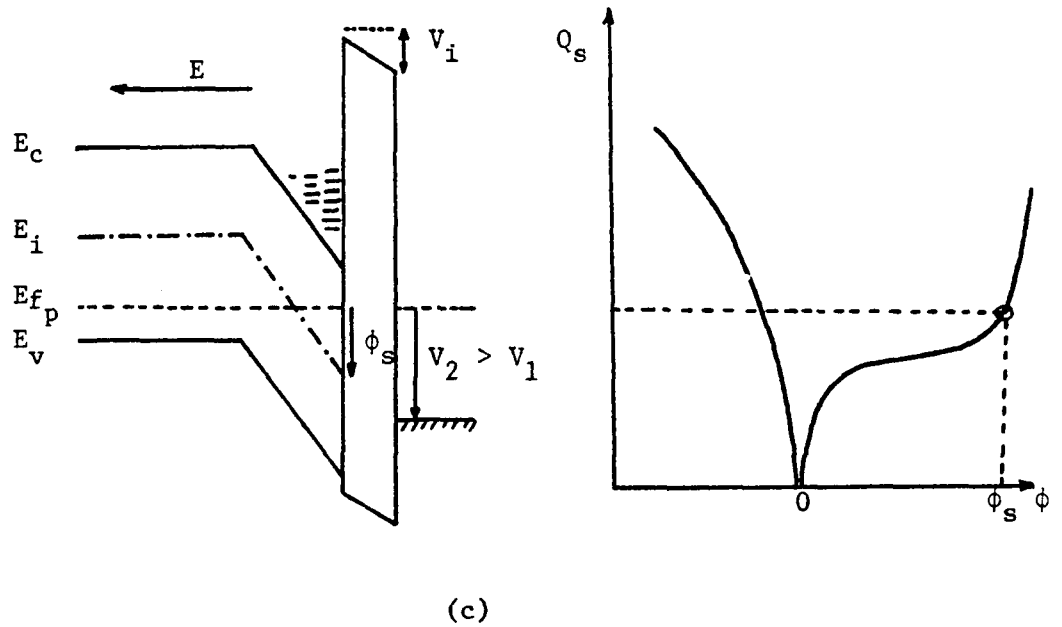


Fig. 2.1 (Continued)

- (c) For an external applied voltage $V_2 > 0$, there is an accumulation of negative charges greater than case (b) at the SiO₂-Si interface.

$$V = V_i + \phi_s \quad (2.2)$$

$$V_i = \text{voltage across insulator (SiO}_2) = \frac{Q_s d}{e_i} = \frac{Q_s}{C_i}$$

e_i = permittivity of SiO₂ region

ϕ_s = semiconductor surface voltage

d = SiO₂ thickness

C_i = SiO₂ capacitance/area

Total capacitance/area versus voltage of the MIS system can be calculated as

$$C = \frac{C_i C_D}{C_i + C_D} \quad (2.3)$$

where the depletion capacitance/area, C_D , is

$$C_D = \frac{dQ_s}{d\phi} = \frac{(1 - \exp(B\phi) + \frac{n_{po}}{p_{po}} (\exp(B\phi) - 1))}{F(B\phi, \frac{n_{po}}{p_{po}})} \quad (2.4)$$

Eq. (2.3) is calculated for the case in which MIS structure is ideal, that is, there is no difference in the semiconductor metal work function, no surface states, no surface state charges, and no impurity charges in the SiO₂ layer exist. A plot of C versus V is shown in Fig. 2.2 for a p-type substrate Si material. Experimental deviations of this C versus V curve will show the presence of fast surface states, impurity charges in SiO₂-Si layer, and surface state charges, Q_{ss} , at the SiO₂-Si interface.

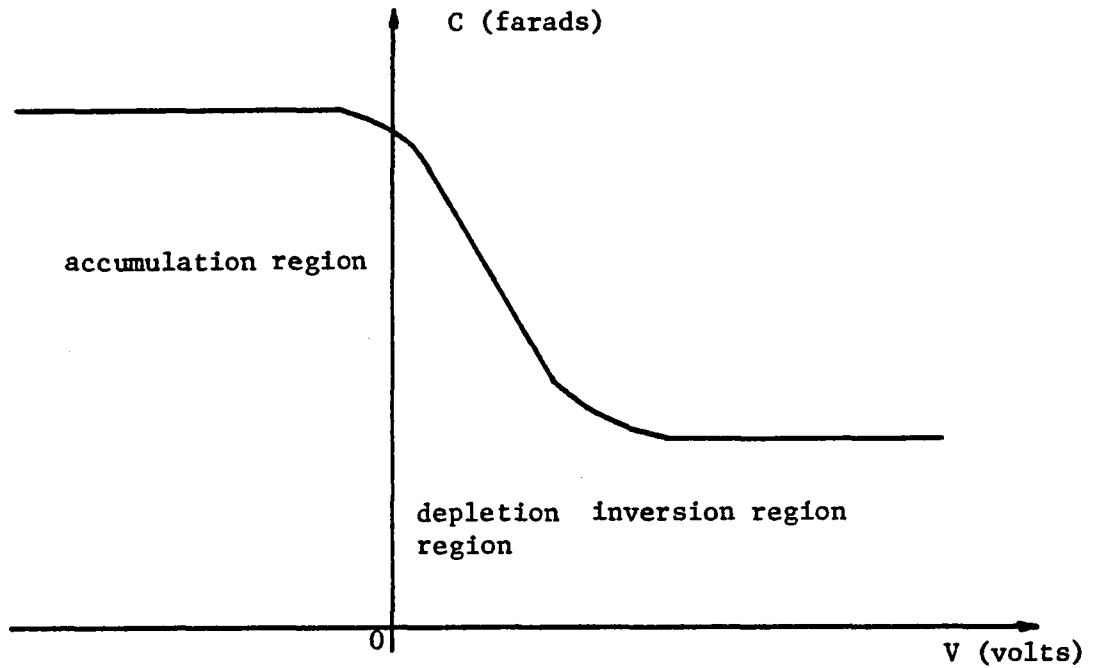


Fig. 2.2 C-V Curve of an MIS System.

The C-V curve shown above is for a p-type Si material. For an n-type Si material, the C-V curve is obtained by a C-axis reflection of Fig. 2.2.

Interpretation of capacitance versus voltage, (C-V), experimental curves of MIS devices are based upon the following criteria:

1. The existence of a work function difference, $\phi_{ms} = \phi_m - \phi_s$, between the metal gate and the silicon material, shifts the experimental C-V curve parallel to the ideal one. The amount of displacement will be equivalent to the amount of ϕ_{ms} difference. Here ϕ_m = work function of metal; ϕ_s = work function of semiconductor. Fig. 2.3 (a) shows this situation.

2. The existence of interface state charges, Q_{ss} , shift the experimental C-V curve parallel to the ideal C-V curve. The direction of displacement indicates the polarity of Q_{ss} . Fig. 2.3 (b) shows this situation.

3. The existence of fast surface states distorts the shape of the C-V curve in the depletion and strong inversion regions. Fig. 2.3 (c) shows this situation.

4. Contamination of the SiO_2 layer shows a parallel symmetric shift of the ideal C-V curve under positive or negative thermal stress treatment.

Experimental Procedure

Procedure for C-V plots of MIS structures consist of three main parts. The anodic oxidation of Si wafers. The metal deposition on SiO_2 layers. Measurements and interpretation of MIS curves.

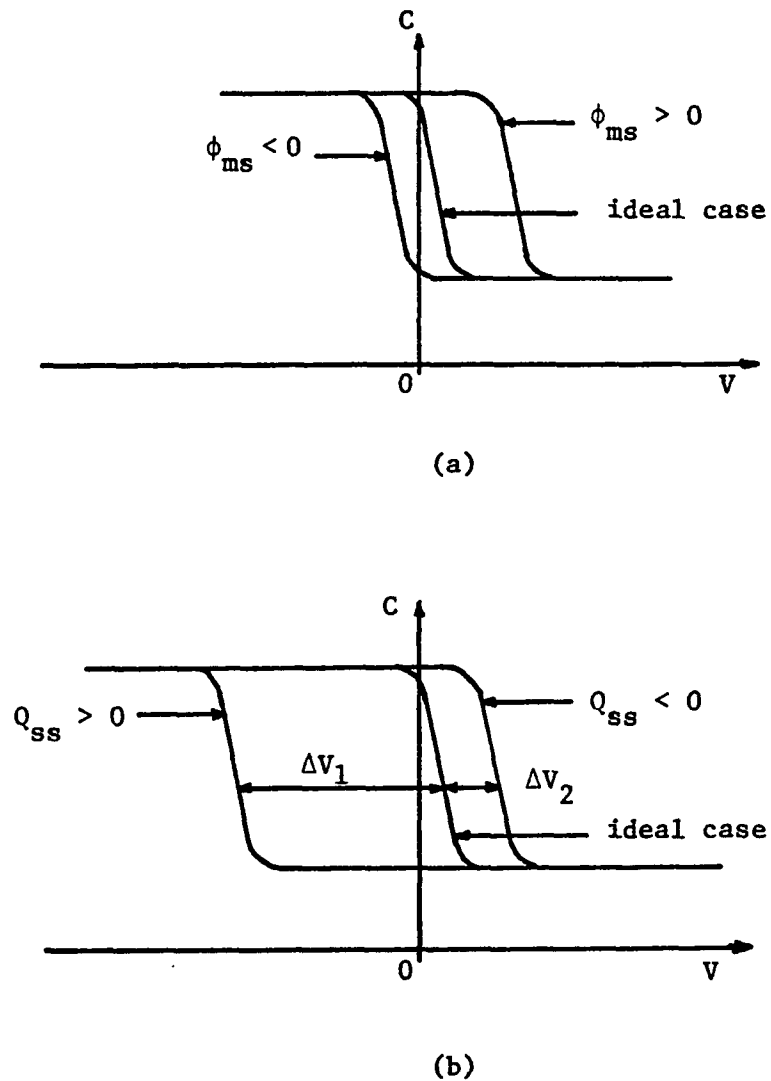
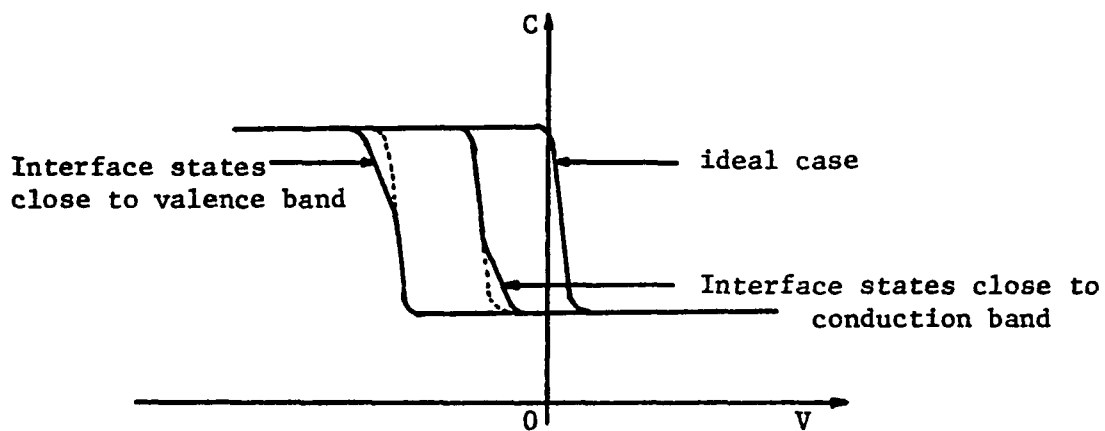


Fig. 2.3 C-V Curves under Different Conditions

- (a) This situation represents the effect on a difference in work functions between the metal electrode and the semiconductor electrode.
- (b) This situation represents the effect of the presence of impurity charges in the SiO_2 region.



(c)

Fig. 2.3 (Continued)

(c) This situation represents the effects of an imperfect SiO_2 -Si interface.

Anodic Oxidation of Si

The method consists of immersing clean Si wafers in an electrolyte solution of potassium nitrate (KNO_3), and ethylene glycol ($\text{C}_2\text{H}_6\text{O}_2$) at different molar concentrations, and applying a direct current (DC) anodization voltage across the metal-electrolyte-semiconductor cell (MES). Fig. 2.4 shows the experimental arrangement of this method. Appendix A contains the cleaning procedure for Si wafers. Preparation method of ethylene glycol solutions are contained in Appendix B. Ethylene glycol is selected as an electrolyte because of its chemical inert nature to Si. Other electrolyte compounds could be used, however. KNO_3 salt is used in the electrolyte to establish a low resistance path for electrons and Si ions across the MES cell under the influence of an external anodization electric field.

Anodic oxide growth is carried out under application of a varying DC forming voltage in such a way that the total current density across the MES cell is kept constant. This variation of V_f is allowed until the desired SiO_2 thickness is reached. After this happens the forming voltage is kept constant in such a way as to allow the current density to decay to a predetermined value. This method of SiO_2 growth inhibits a high density of states at the SiO_2 -Si interface (Revez 1967).

Several molar concentrations of KNO_3 in ethylene glycol are used in this experiment. Variation of these molar concentrations allows the initial forming voltage, of the Si electrode, to vary accordingly.

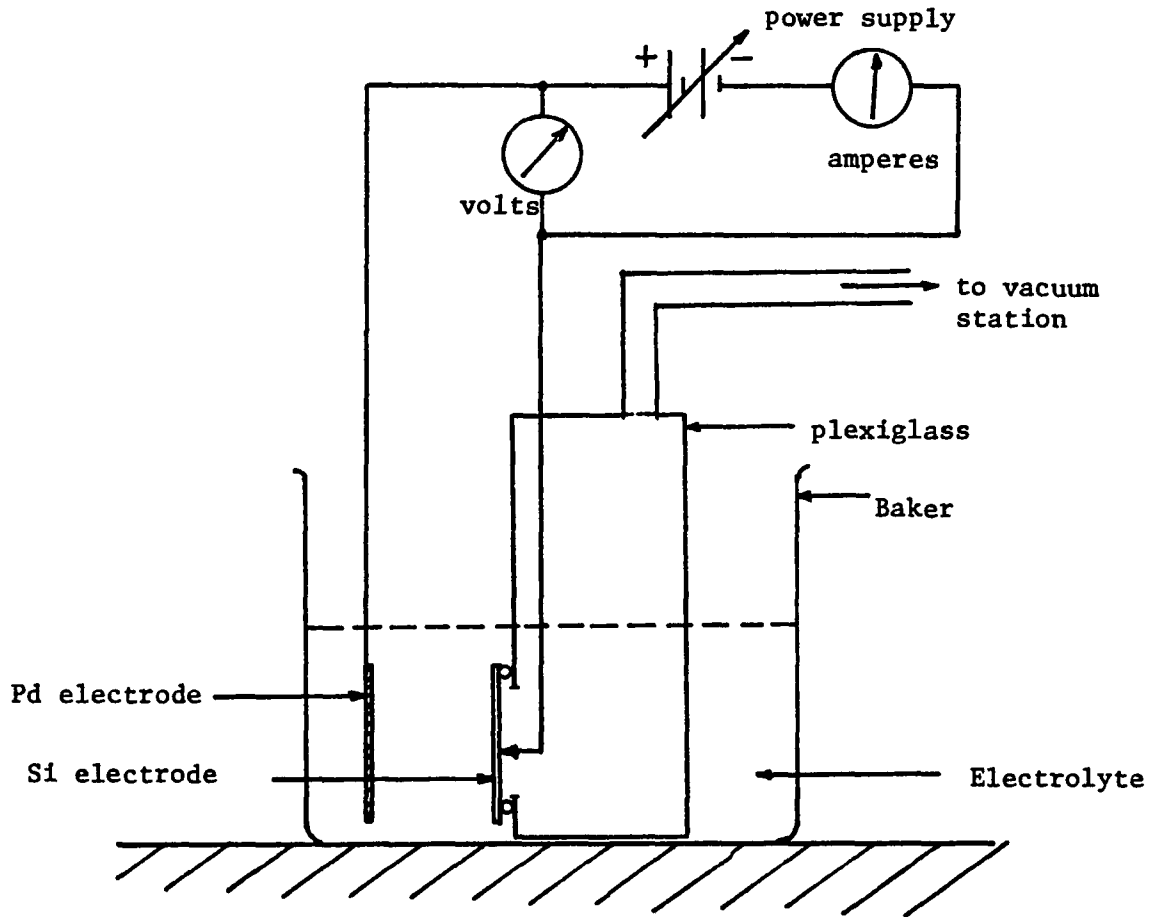


Fig. 2.4 Experimental Arrangement for Anodic Oxidation of Si

Metal Deposition

Aluminum metal is used for the electrode in MIS devices. Deposition of aluminum (Al) on top of SiO_2 grown layers is made in a vacuum station at pressures $< 10^{-6}$ torr. The evaporation is carried out at $\approx 700^\circ\text{C}$. The SiO_2 -Si substrate temperature is kept $\approx 100^\circ\text{C}$. Aluminum electrodes on MIS devices have "key hole" shapes as shown in Fig. 2.5. The central dot acts as the active area of MIS capacitors. The external ring with a contact pad is used to avoid surface currents on the SiO_2 layer.

Measurement of C-V Curves

An alternating current (AC) voltage is used to measure the capacitance of MIS devices. The frequency of this signal is 100 khz. It is high enough to prevent the minority carriers, in the inversion region of the semiconductor surface, from following this variation. A direct current (DC) voltage is added to the ac signal voltage. This dc voltage changes the value of the electrostatic potential at the surface of the semiconductor and thus the capacitance of the device.

The steps for C-V measurements are as follows:

1. At room temperature set a dc bias voltage in the metal electrode of 50 volts with respect to the semiconductor.
2. Allow the dc bias to change from 50 to -50 volts and measure the change in capacitance in an X-Y plotter.
4. Allow the dc bias to change from -50 to 50 volts and measure the change in capacitance. This set of curves is used to

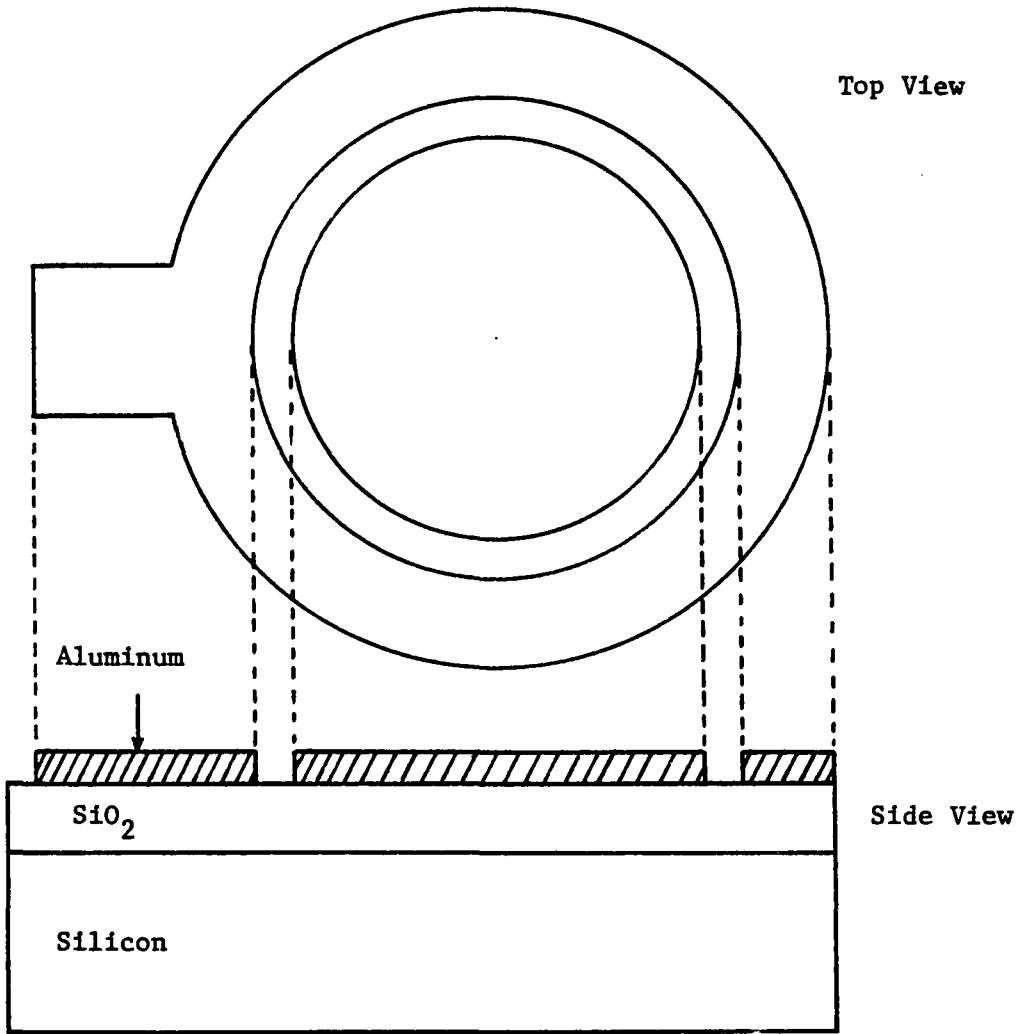


Fig. 2.5 Geometrical Arrangement for an MIS Capacitor
(Not to scale)

detect the presence of surface states, and surface state charges (fixed charges). The value of the charge density and surface density is given by

$$\frac{Q_{ss}}{q} = \frac{K\epsilon_0(V + \phi_{ms})}{qd} \text{ (m}^{-2}\text{)} \quad (2.5)$$

where

d = SiO₂ thickness

K = dielectric constant of SiO₂

ϵ_0 = electrical permittivity of free space

V = displacement of C-V curve with respect to the ideal case.

ϕ_{ms} = metal semiconductor work function difference

If no distortion exists on the experimental C-V curves, Eq.

(2.5) gives the value of the surface charge only.

4. At a temperature of 250°C, set the dc bias voltage on the metal electrode for 10 volts and a period of 5 minutes.
5. Allow the temperature of MIS capacitor to decrease to room temperature while maintaining the 10 volts bias voltage.
6. At room temperature measure C-V curves by changing the dc bias from 50 to -50 volts.
7. At a temperature of 250°C set a dc bias voltage on the metal electrode of -10 volts for a period of 5 minutes.
8. Allow temperature of the MIS capacitor to decrease to room temperature while maintaining the -10 bias voltage.
9. At room temperature measure C-V curves by changing dc bias from -50 to 50 volts.

This set of curves is used to detect the presence of SiO_2 impurity contamination (mobile carriers). Calculation of the amount of impurity contamination in SiO_2 is not of interest in this experiment.

Materials Used

Silicon wafers used in this work are p-type with resistivities of $0.1 \Omega\text{m}$ and crystal orientation $\langle 111 \rangle$. Dimensions of the Si wafers are $4 \times 10^{-4} \text{ m}^2$ with thicknesses of $H = 250 \mu\text{m}$.

The molar concentration of KNO_3 salts dissolved in ethylene glycol are: 0.02 M, 0.04 M, 0.06 M, and 0.08 M.

The metal electrode employed in the MES cell consist of a steel plate of 0.02 by 0.06 m. on which a layer of approximately 10,000 Å of palladium (Pd) has been deposited by vacuum evaporation method at a pressure of 10^{-6} torr. The temperature of Pd evaporation occurs at about 1600°C .

The Si electrode wafer holder consists of a plexiglass rectangular box with a spring copper contact attached to one of the side faces. The sealing ring between the Si wafer and the box is made of silicon rubber able to stand temperatures of 200°C . The Si wafer was held by means of vacuum suction. Fig. 2.6 shows the experimental set up for measuring C-V curves in MIS devices.

Results

Measurements of C-V curves were made on a total of 30 Si wafers. Each wafer consists of about 20 MIS capacitors. Data from

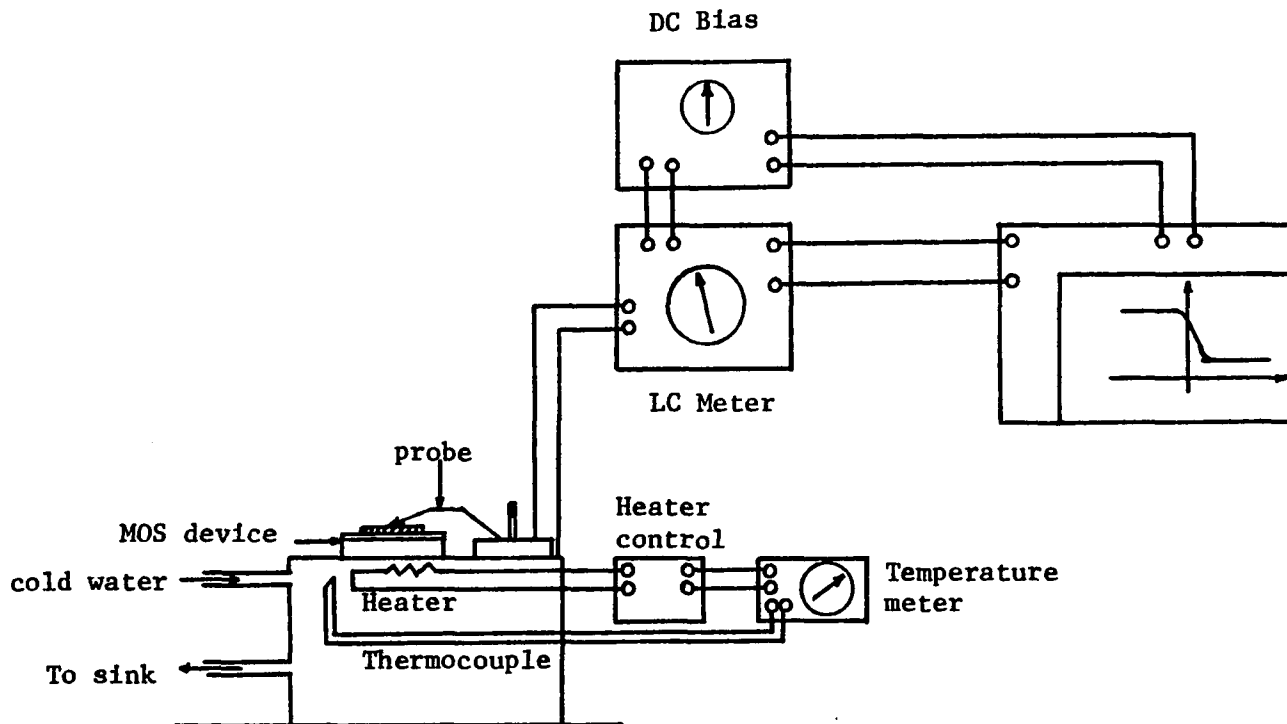


Fig. 2.6 Experimental Arrangement for the Measurement of the C-V Characteristics of Anodic SiO_2 MOS capacitors.

5 capacitors per wafer were taken; one capacitor was selected from the center and the other from the side of a wafer. The electrolyte used in each anodic growth was freshly made; this situation ensures reproducibility in the growth conditions.

The first SiO_2 batch was grown under the conditions indicated in Table 2.1. Results on the measured Q_{ss} of the described batch are given in Table 2.2. Data in Table 2.2 indicates a significant increase of positive Q_{ss} in the SiO_2 -Si interface as the anodic current is increased through the MES cell.

Table 2.1 Anodic Silicon Dioxide Growth Conditions for Several Si Wafers

Wafer Number	Anodic Current	Molar Concentration	Forming Voltage	Oxide Thickness
5	25 mA	0.02 M	250 v	1250 Å
8	25 mA	0.02 M	250 v	1250 Å
9	25 mA	0.02 M	250 v	1300 Å
10	25 mA	0.02 M	250 v	1350 Å
4	50 mA	0.02 M	250 v	1150 Å
6	50 mA	0.02 M	250 v	1150 Å
7	50 mA	0.02 M	250 v	1150 Å

Table 2.2 Density of Surface State Charges of Several MIS Capacitors

Wafer Number	Anodic Current	$Q_{ss}/q(m^{-2})$	Average $Q_{ss}/q(m^{-2})$
5	25 mA	3.13×10^{15}	
8	25 mA	4.11×10^{15}	5.54×10^{15}
9	25 mA	6.74×10^{15}	
10	25 mA	7.85×10^{15}	
4	50 mA	7.93×10^{15}	
6	50 mA	8.01×10^{15}	8.61×10^{15}
7	50 mA	9.91×10^{15}	

A second batch of SiO_2 growth was made to observe the effect of SiO_2 thickness on Q_{ss} generation. Table 2.3 shows the growth conditions. Results on the measured Q_{ss} of the second batch are given in Table 2.4.

Table 2.3 Anodic Silicon Dioxide Growth Conditions for the Second Batch of Si Wafers

Wafer Number	Anodic Current	Molar Concentration	Forming Voltage	Oxide Thickness
11	25 mA	0.02 M	400 v	2200 Å
13	25 mA	0.02 M	400 v	1850 Å
12	50 mA	0.02 M	400 v	1850 Å

Table 2.4 Density of Surface State Charge of the Second Batch of MIS Capacitors

Wafer Number	Anodic Current	$Q_{SS}/q(m^{-2})$	Average $Q_{SS}/q(m^{-2})$
11	25 mA	5.39×10^{15}	4.65×10^{15}
13	25 mA	3.91×10^{15}	
12	50 mA	4.19×10^{15}	4.19×10^{15}

Data of Q_{SS} in Table 2.4 indicates no significant change in the surface charge generation at the SiO_2 -Si interface as the current is increased from 25 to 50 mA.

From the above observations, an increase in Q_{SS} at the SiO_2 -Si interface is possible by increasing the anodic current as much as possible; however, it was found that anodic current densities above $1.5 \times 10^2 A/m^2$ produce porous SiO_2 . All MIS capacitors made from porous SiO_2 show a short circuit condition. Data from Tables 2.2 and 2.4 indicates that the amount of Q_{SS} generated under such conditions is below that reported in the literature (Raider and Berman 1978).

A second optimization parameter considered was the electrolyte resistance (molar concentration of KNO_3), therefore a third batch was made; its growth conditions are summarized in Table 2.5. Results on the measurements of Q_{SS} of this batch are given in Table 2.6.

Data of Q_{SS} in Table 2.6 indicates again an increase in Q_{SS} as the anodic current is increased. Also, it shows that decreasing

Table 2.5 Anodic Silicon Dioxide Growth Conditions for the Third Batch of Silicon Wafers

Wafer Number	Anodic Current	Molar Concentration	Forming Voltage	Oxide Thickness
22	25 mA	0.04 M	250 v	1400 Å
24	25 mA	0.04 M	250 v	1470 Å
21	50 mA	0.04 M	250 v	1450 Å
23	50 mA	0.04 M	250 v	2300 Å

Table 2.6 Density of Surface State Charge of the Third Batch of MIS Capacitors

Wafer Number	Anodic Current	$Q_{ss}/q \text{ m}^{-2}$	Average $Q_{ss}/q \text{ cm}^{-2}$
22	25 mA	9.59×10^{15}	9.6×10^{15}
24	25 mA	9.70×10^{15}	
21	50 mA	1.73×10^{16}	1.45×10^{16}
23	50 mA	1.16×10^{16}	

electrolyte resistance it is possible to increase Q_{ss} . For completeness, as in 0.02 M batch, another batch of 0.04 M was studied with thicker SiO_2 layer. Growth conditions are shown in Table 2.7.

Results of the measured Q_{ss} of wafers from Table 2.7 are given in Table 2.8. These results show no significant change in Q_{ss} by

Table 2.7 Anodic Silicon Dioxide Growth Conditions for the 4th Batch of Silicon Wafers

Wafer Number	Anodic Current	Molar Concentration	Forming Voltage	Oxide Thickness
1	25 mA	0.04 M	400 v	2150 Å
20	25 mA	0.04 M	400 v	2350 Å
2	50 mA	0.04 M	400 v	2250 Å
17	50 mA	0.04 M	400 v	2600 Å
19	50 mA	0.04 M	400 v	2450 Å

Table 2.8 Density Surface State Charge of the 4th Batch of MIS Capacitors

Wafer Number	Anodic Current	$Q_{SS}/q \text{ m}^{-2}$	Average $Q_{SS}/q \text{ m}^{-2}$
1	25 mA	1.41×10^{16}	1.6×10^{16}
20	25 mA	1.78×10^{16}	
2	50 mA	5.51×10^{15}	1.41×10^{16}
17	50 mA	1.68×10^{16}	
19	50 mA	2.01×10^{16}	

increasing anodic current from 25 to 50 mA. This situation resembles that of the 0.02 M batches.

Further decrease in electrolyte resistance was studied to see its effect on the surface charge generation. For this situation Table 2.9 lists the growth conditions of this batch. Also Table 2.10 shows the results of Q_{ss} generation for this batch.

Table 2.9 Anodic Silicon Dioxide Growth Conditions for the 5th Batch of Silicon Wafers

Wafer Number	Anodic Current	Molar Concentration	Forming Voltage	Oxide Thickness
27	25 mA	0.06 M	250 v	1500 Å
34	25 mA	0.06 M	250 v	1300 Å
25	50 mA	0.06 M	250 v	1560 Å
28	50 mA	0.06 M	250 v	1300 Å

Table 2.10 Density of Surface State Charge of the 5th Batch of MIS Capacitors

Wafer Number	Anodic Current	$Q_{ss}/q \text{ m}^{-2}$	Average $Q_{ss}/q \text{ m}^{-2}$
27	25 mA	1.80×10^{16}	1.75×10^{16}
34	25 mA	1.69×10^{16}	
25	50 mA	2.04×10^{16}	2.02×10^{16}
28	50 mA	2.00×10^{16}	

Data from Table 2.10 shows also that Q_{SS} generation increases with anodic current. This amount of Q_{SS} is higher as that of Table 2.6 in which both batches have, on the average, the same SiO_2 thickness.

In an analogous way, as in batches from Tables 2.3 and 2.7, SiO_2 was grown on two wafers at 380 volts of forming voltage (thicker oxide). Growth conditions of these wafers are listed in Table 2.11.

Results in Q_{SS} from the above two wafers are given in Table 2.12.

Table 2.11 Anodic Silicon Dioxide Growth Conditions for the 6th Batch of Silicon Wafers

Wafer Number	Anodic Current	Molar Concentration	Forming Voltage	Oxide Thickness
30	25 mA	0.06 M	380 v	2400 Å
26	50 mA	0.06 M	380 v	2300 Å

Table 2.12 Density of Surface State Charge of the 6th Batch of MIS Capacitors

Wafer Number	Anodic Current	$Q_{SS}/q \text{ m}^{-2}$	Average $Q_{SS}/q \text{ m}^{-2}$
30	25 mA	1.86×10^{16}	1.86×10^{16}
26	50 mA	1.70×10^{16}	1.70×10^{16}

Above results show that a charge in Q_{SS} using 25 or 50 mA is not as sensitive as in the last batches. Also Q_{SS} is not as high as that on Table 2.10; however, the 0.06 M batch generates, on the average, higher Q_{SS} than those of the 0.04 M batches. For this reason the following batch was made hoping to increase Q_{SS} by lowering further the resistance of the electrolyte. The growth conditions of this batch are given in Table 2.13. Results of the 7th batch of MIS capacitors are given in Table 2.14.

Table 2.13 Anodic Silicon Dioxide Growth Conditions for the 7th Batch of Silicon Wafers

Wafer Number	Anodic Current	Molar Concentration	Forming Voltage	Oxide Thickness
14	25 mA	0.08 M	250 v	1450 Å
15	50 mA	0.08 M	250 v	1750 Å
35	25 mA	0.08 M	380 v	2550 Å
36	50 mA	0.08 M	380 v	1900 Å

Table 2.14 Density of Surface State Charge of the 7th Batch of MIS Capacitors

Wafer Number	Anodic Current	$Q_{ss}/q \text{ m}^{-2}$	Average $Q_{ss}/q \text{ m}^{-2}$
14	25 mA	1.75×10^{16}	1.75×10^{16}
15	50 mA	1.78×10^{16}	1.78×10^{16}
35	25 mA	1.59×10^{16}	1.59×10^{16}
36	50 mA	1.58×10^{16}	1.58×10^{16}

Data from Table 2.14 indicate very small Q_{ss} increase in wafer 15 from that of wafer 14. Both wafers have thinner oxides than wafers 35 and 36. These last two wafers do not show high relative percentage change in Q_{ss} generation as those from batches 0.02 M, 0.04 M, and 0.06 M. SiO_2 grown layers, using 0.08 M electrolytes, show visible surface contamination of KNO_3 salt crystals. C-V measurements in this batch were difficult to carry out due to high surface currents on the SiO_2 layers.

Discussion of Results

The anodic oxidation of Si is known not to be a very efficient process. Most of the current in the MES cell is 97-99% electronic. Various models proposed in the literature indicate that anodic oxidation of Si, with electric fields $< 1.5 \times 10^9$ volts/m across the SiO_2 , occurs by a transport mainly of OH^- radicals, present in the electrolyte, through the SiO_2 layer and then to the Si surface where they

react with this surface to form new SiO_2 . Thus, the rate of oxide generation is proportional to the anodic current density through the MES cell. For electric fields $> 1.5 \times 10^9$ volts/m the oxidation process is mainly due to field enhancement diffusion of Si ions through the SiO_2 layer and into the electrolyte- SiO_2 interface where they react with oxidizing species (Revez 1973).

To maintain a constant current through the SiO_2 layer as the oxide layer grows thicker, the forming voltage must increase. Usually, it is found experimentally that the variation of the forming voltage with respect to time is linear as well as the variation of the oxide thickness with respect to time. Fig. 2.7 shows typical voltage versus time and oxide thickness versus time curves. Assuming that the electric field across the SiO_2 layer is constant, the variation of the forming voltage and oxide thickness with respect to time are related as

$$\frac{dV}{dt} = E \frac{dx}{dt} \quad (2.6)$$

where

E = Electric field through SiO_2

x = SiO_2 thickness

V = Forming voltage

From Eq. (2.6) it is possible to calculate the order of magnitude of the electric field in SiO_2 growth. Typical cases are

$$E_{\min} = \frac{dV/dt}{dx/dt} = 8.79 \times 10^8 \text{ v/m (wafer 17)}$$

$$E_{\max} = \frac{dV/dt}{dx/dt} = 2.14 \times 10^9 \text{ v/m (wafer 13)}$$

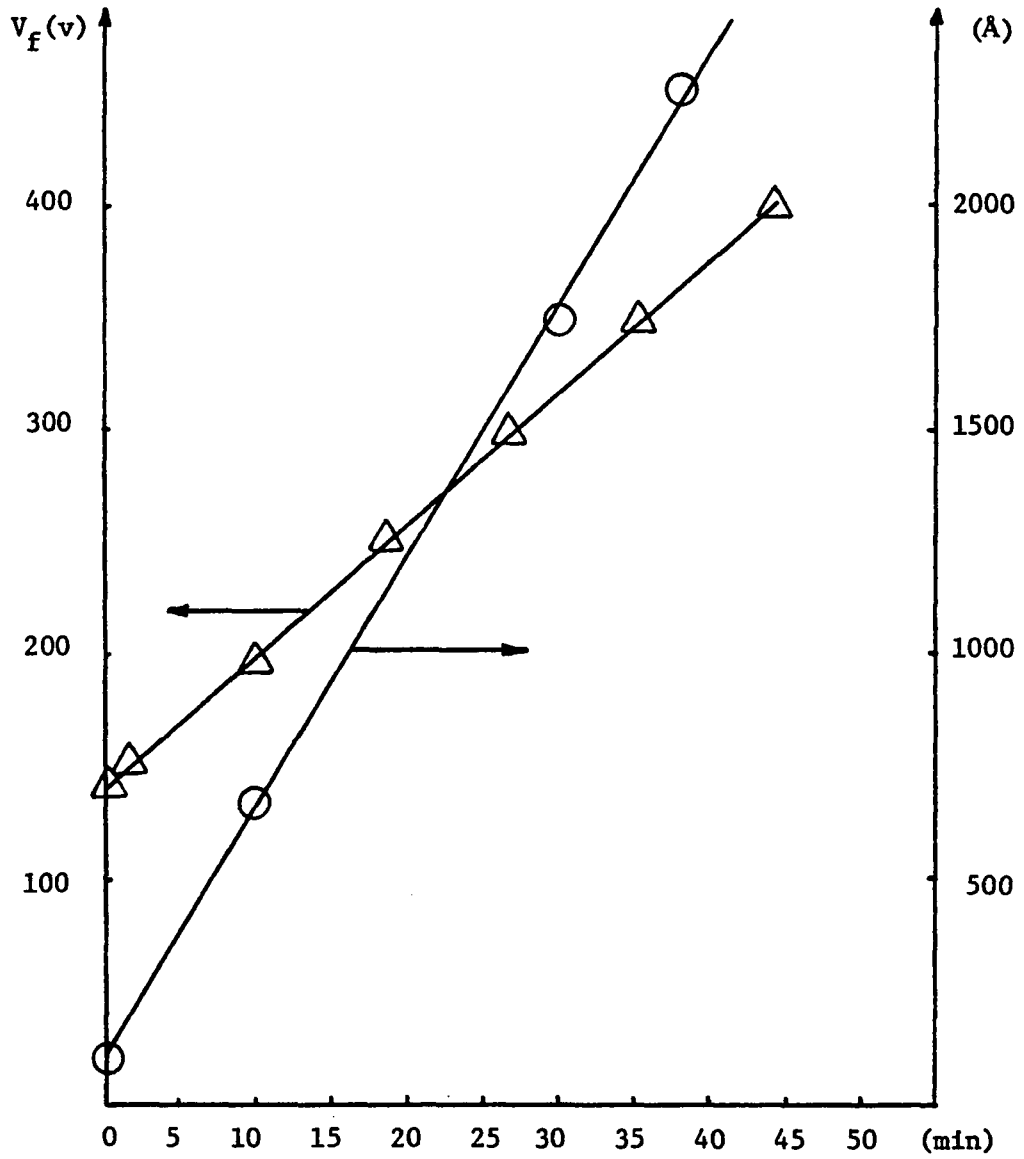


Fig. 2.7 Typical Forming Voltage and SiO_2 Thickness versus Growing Time Curves

Using Eq. (2.6) and data from Appendix C, the average value of E field in anodic oxide growth is

$$\langle E \rangle = 1.65 \times 10^9 \text{ v/m}$$

To visualize and facilitate the discussion about results in Q_{SS} for different growing conditions see Fig. 2.8, the Q_{SS} generation versus molar concentration at different anodic currents.

Referring to Fig 2.8, plots of these curves were made by taking the average value of Q_{SS} of the MIS capacitors with SiO_2 layers grown in similar conditions. It is easily seen from this figure, that Q_{SS} generation depends on two factors: First, the amount of Q_{SS} generated at the SiO_2 -Si interface is influenced by the electrical resistance of the electrolyte (molar concentration of KNO_3). Second, an increase in Q_{SS} generation is produced by an increase in anodic current through the MES cell. An explanation of the first influencing factor can be made by calculating the average electric field across the SiO_2 layers using Eq. (2.6) and data from Appendix C. These results are shown in Table 2.15.

From data in Table 2.15, one can argue that: For wafers with anodic current densities of $1.25 \times 10^2 \text{ A/m}^2$ and the same electrolyte concentration, the average electric field across the SiO_2 layers has values $< 1.5 \times 10^9 \text{ v/m}$. This indicates that the anodization process under these circumstances is due mainly to field enhanced diffusion of OH^- ions through the SiO_2 layers toward the SiO_2 -Si interface. This oxidation process, resembles that explained for thermal oxides (Raider and Berman 1978). For wafers with an anodic current density of

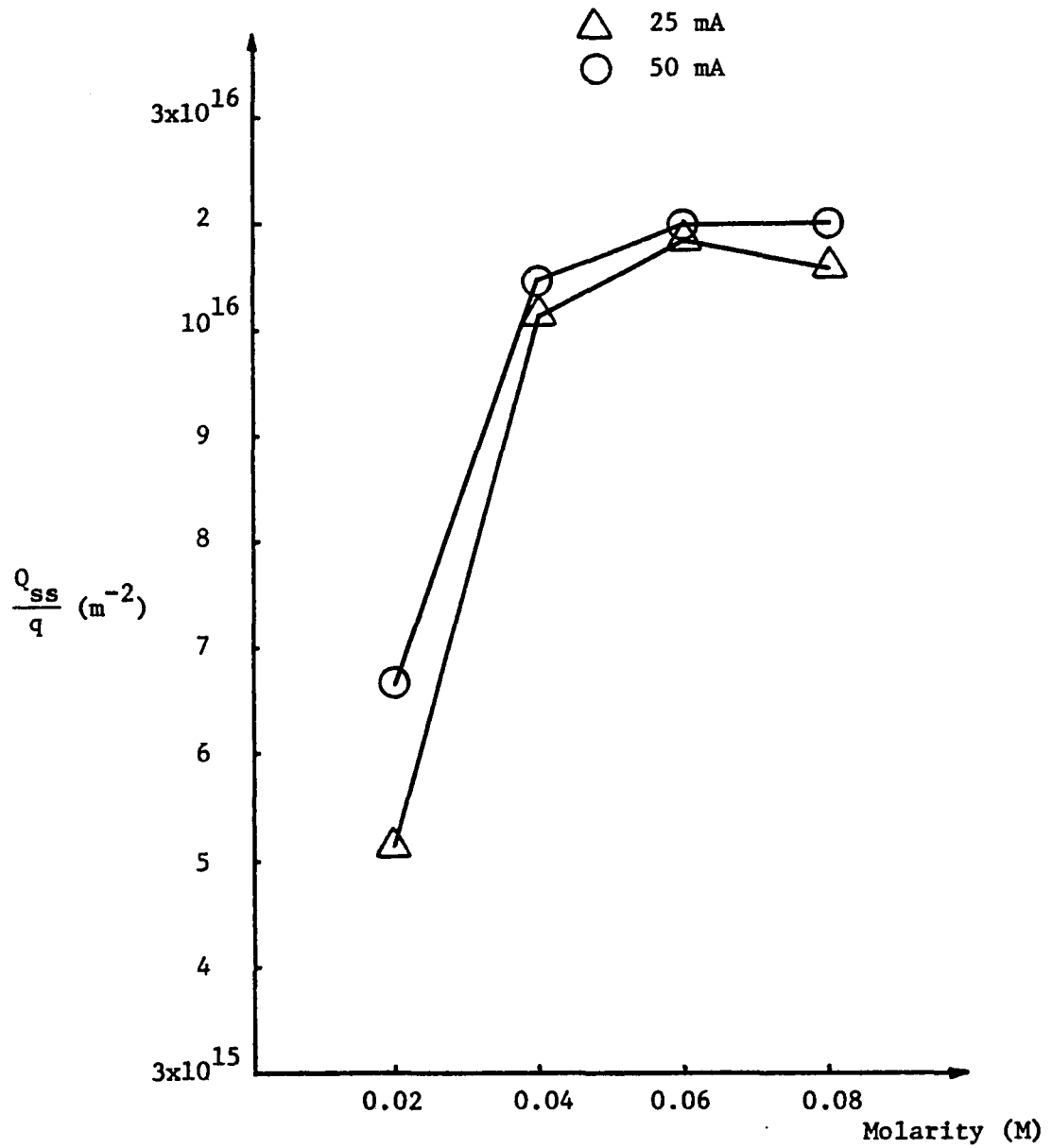


Fig. 2.8 Average Q_{ss} Generation versus Different Molarity Growth Conditions

Table 2.15 Comparison between the Average Electric Field and the Average Surface Charge Generation with Different Oxide Growth Conditions

Molar Concentration	Anodic Current	Average Electric Field	Average Q_{ss}/q
0.02 M	25 mA	2.00×10^9 v/m	$5.10 \times 10^{15} \text{ m}^{-2}$
0.02 M	50 mA	1.39×10^9 v/m	$6.40 \times 10^{15} \text{ m}^{-2}$
0.04 M	25 mA	1.61×10^9 v/m	$1.28 \times 10^{16} \text{ m}^{-2}$
0.04 M	50 mA	1.00×10^9 v/m	$1.43 \times 10^{16} \text{ m}^{-2}$
0.06 M	25 mA	1.81×10^9 v/m	$1.81 \times 10^{16} \text{ m}^{-2}$
0.06 M	50 mA	1.43×10^9 v/m	$1.86 \times 10^{16} \text{ m}^{-2}$
0.08 M	25 mA	1.73×10^9 v/m	$1.67 \times 10^{16} \text{ m}^{-2}$
0.08 M	50 mA	1.43×10^9 v/m	$1.94 \times 10^{16} \text{ m}^{-2}$

62.5 A/m^2 and the same electrolyte concentration, the average electric field across the SiO_2 layers has values $> 1.5 \times 10^9$ v/m. This indicates that the anodization process under these circumstances is due predominantly to field enhanced diffusion of Si^+ ion through the SiO_2 layers toward the SiO_2 -electrolyte interface. This oxidation process, although not well understood, generates lower Q_{ss} charges at the SiO_2 -Si interface.

A figure of merit in this experiment is the percentage change in Q_{ss} charges using two different anodic current densities. A plot of this figure of merit versus concentration of KNO_3 in the electrolyte is shown in Fig. 2.9. This figure shows that SiO_2 growth using 0.02 M

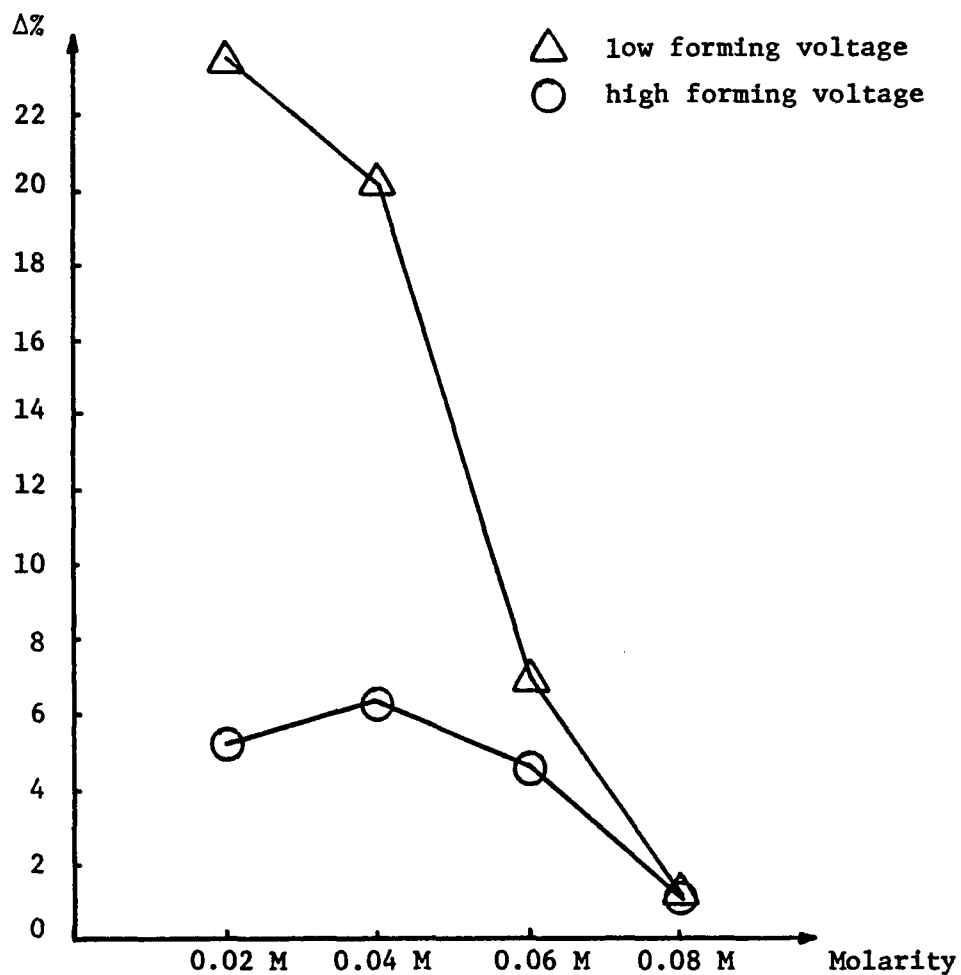


Fig. 2.9 Percentage in change in Q_{ss} Generation versus Different Molarity Growth Conditions

$$\Delta\% = \frac{Q_{ss}(50 \text{ mA}) - Q_{ss}(25 \text{ mA})}{Q_{ss}(50 \text{ mA}) + Q_{ss}(25 \text{ mA})} \times 100$$

electrolyte is very sensitive to Q_{SS} charge generation under two different forming voltage values (different oxide thicknesses). As molar concentration in the electrolyte increases, this variation in Q_{SS} difference decreases considerably to a such value that anodic oxide growth made with 0.08 M electrolyte produces about the same density of Q_{SS} charges at different forming voltages. It is seen also from Fig. 2.9, that the sensitivity of Q_{SS} generation is small when SiO_2 is grown with high forming voltages.

Summary

Surface charge generation at the interface of an anodic SiO_2 -Si system was investigated. The anodic growth was made with several different concentrations of KNO_3 salts in a non-aqueous electrolyte, ethylene glycol. Measurements of the surface charge, Q_{SS} , were made using C-V curves of MIS capacitors. It was found that Q_{SS} charge generation depends on two factors: The electric resistance of the electrolyte (molar concentration) and the anodic current through a Metal-Electrolyte-Semiconductor cell.

The dependence of Q_{SS} charge on molar concentration is such that it increases as the concentration of KNO_3 is increased. There is a limit to this charge generation, however, its value saturates to a density value of $Q_{SS}/q = 2 \times 10^{16} \text{ m}^{-2}$ when the electrolyte concentration reaches the value of 0.08 M.

The dependence of Q_{SS} charge on the anodic current is such that it increases as the anodic current through the MES cell is

increased. There is a limit value for the Q_{ss} charge generation. Its value is limited by the amount of anodic current that can produce non-porous SiO_2 layers. It was found experimentally that the value of this anodic current density is of the order of $1.5 \times 10^2 \text{ A/m}^2$.

CHAPTER 3

THEORETICAL QUANTUM EFFICIENCY

Quantum efficiency of the non-amplifying anodic SiO₂-Si light detector, as discussed in Chapter 1, depends on the ratio of total current density flowing across the device to the amount of mono-energetic photons falling onto the active area of the detector. It is the purpose of this chapter to calculate such efficiency. These calculations are based upon the solution of Eq. (1.9) with Eqs. (1.10) and (1.11) as boundary conditions. Some of the experimental data found in Chapter 2 will be used in these calculations.

A Simplified Model

Interface behavior of the electrostatic potential at the surface of a semiconductor, due to the presence of positive charges on the surface of the semiconductor, can be easily analyzed using the appropriate model employed in studying one-sided step p-n junctions. This model is sometimes called the "depletion approximation" (Grove 1967). Using the "depletion approximation" model, the spatial dependence of the electric field and electrostatic potential are given as

$$E(x) = E_{\max} \left(1 - \frac{x}{w_m}\right) \quad (3.1)$$

$$\phi(x) = \phi_s \left(1 - \frac{x}{w_m}\right)^2 \quad (3.2)$$

where

$E(x)$ = electric field in the semiconductor

$\phi(x)$ = electrostatic potential inside the semiconductor

E_{\max} = electric field value at the surface of the semiconductor

$$= \frac{qN_A w_m}{K_s e_0}$$

ϕ_s = electrostatic potential value at the surface of the semiconductor

x = distance from the surface into the bulk of the semiconductor

$$w_m = \text{maximum width of depletion region} = \frac{(2K_s e_0 \phi_s)^{1/2}}{qN_A}$$

N_A = impurity acceptor concentration in the semiconductor

The spatial dependence of the electric field and the electrostatic potential given by Eqs. (3.1) and (3.2) respectively, will be used in Eq. (1.9) to find approximate solutions to them. The values of E_{\max} and ϕ_s depend on the amount of charged states at the surface of the semiconductor. In the present case, the presence of surface state charges at the anodic SiO_2 -Si interface will be considered. Their density value will be taken from the experimental data found in Chapter 2.

Calculation of Parameters

The wave length dependence of the reflection coefficient, R , which appears in Eq. (1.9), takes into account the interference effects

created by the light falling onto the three layer system, air-SiO₂-Si. Its value is calculated from the equation (Hovel 1975).

$$R = \frac{r_1^2 + r_2^2 + 2r_1r_2\cos\theta}{1 + r_1^2r_2^2 + 2r_1r_2\cos\theta} \quad (3.3)$$

where r_1 , r_2 are the Fresnel coefficients given by

$$r_1 = \frac{n_0 - n_1}{n_0 + n_1} \quad (3.4a)$$

$$r_2 = \frac{n_1 - n_2}{n_1 + n_2} \quad (3.4b)$$

$$\theta = \frac{2 n_1 d_1}{\lambda} \quad (3.4c)$$

and

n_0 = index of refraction of air

n_1 = index of refraction of SiO₂

n_2 = index of refraction of Si

d_1 = thickness of SiO₂ layer

λ = wavelength of incident light

Eq. (3.3) assumes a normal incidence of radiation on the SiO₂-Si detector. To show the wavelength dependence of R, Table 3.1 contains the wavelength variation of n_1 , and n_2 for several Hg lines. Fig. 3.1 shows the wavelength dependence of (1-R) for the interface air-SiO₂-Si for a given SiO₂ thickness. The composite data in Table 3.1 is taken from Schmidt (1969), and Zaghloul, Azzam and Bashara (1978).

Table 3.1 Wavelength Variation of the Indexes of Refraction of SiO₂ and Si

Wavelength (Å)	2537	3131	3341	3650	4046	4358	5461	5657	6683	7371	8097	8723
n ₁ (SiO ₂)	1.5	1.487	1.48	1.475	1.47	1.43	1.45	1.449	1.447	1.445	1.442	1.440
n ₂ (Si)	1.67	4.9	5.06	6.63	5.63	4.83	4.07	3.99	3.78	3.69	3.60	3.58
K(Si)	3.59	3.63	3.04	2.74	0.29	0.116	0.033	2.43 x10 ⁻²	1.44 x10 ⁻²	9.88 x10 ⁻³	5.18 x10 ⁻³	3.33 x10 ⁻³

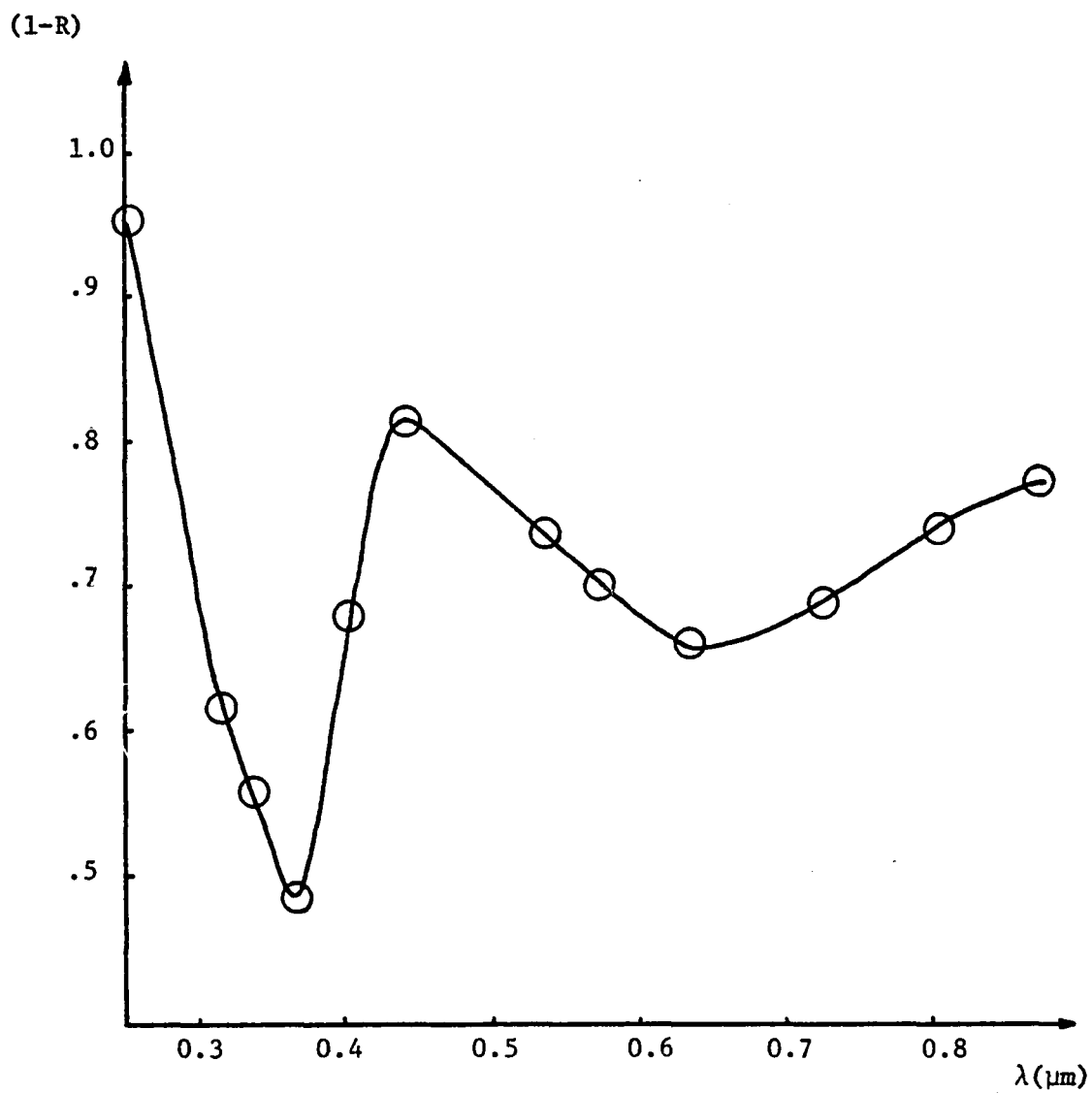
SiO_2 Thickness = 2330 Å

Fig. 3.1 $(1-R)$ Coefficient versus Wavelength of an SiO_2 -Si System

Table 3.2 shows the diffusion and life time of electrons and holes in the SiO₂-Si light detector. This is taken from Salter and Thomas (1975).

Table 3.2 Typical Parameters of a .10 ohm x m p-type Si Material

Parameter	Holes	Electrons
D	6.0 cm ² /sec	40 cm ² /sec
t	10 ⁻⁸ sec	8x10 ⁻⁶ sec

The induced field p-n junction can be calculated from Eq. (1.5) in Chapter 1. The value of x_j depends on the equilibrium electrostatic potential ϕ_p and the electrostatic potential ϕ_s at the surface of the Si material. The former depends on the electrical resistivity of the material. The latter will depend on the density of surface state charge on the SiO₂-Si interface. In the present calculations, the same type of Si wafer material will be used as those found in Chapter 2 with typical values of $\phi_p = 0.31$ volts. The standard value of $\phi_s = 0.83$ volts is taken from the experimental data in Chapter 2 (wafer 1-1). These values of ϕ_p and ϕ_s are used to calculate x_j , using Eq. (1.5), as

$$x_j = \int_{0.31}^{0.83} \frac{qL_D}{2KT} F^{-1} \left(B\phi, \frac{n_{p0}}{p_{p0}} \right) d\phi \approx 0.274 \mu\text{m}.$$

However, if Eq. (3.2) is used

$$x_j = W_M (1 - \sqrt{\phi_p/\phi_s}) \approx 0.286 \text{ } \mu\text{m}.$$

The different methods of calculating x_j , represent a change of 2.14%. For consistency in the calculations of the quantum efficiency of the SiO₂-Si device, the value of x_j from Eq. (3.2) will be used in these calculations.

Current Density Calculations

Solution of the Eq. (1.9a) with boundary conditions given by Eq. (1.11) resembles the boundary value problem encountered in diffused p-n junction detectors. The diffusion current solution for this case is given, for example, Hovel (1975).

$$J_e = - \frac{q\phi_o \alpha L_e (1-R)}{(\alpha^2 L_e^2 - 1)} \exp(-\alpha x_j) \frac{[\text{Cos h}(\frac{H}{J_e}) - \exp(-\alpha H)]}{\text{Sin h}(\frac{H}{L_e})} \quad (3.5a)$$

where

$$L_e = (D_e \tau_e)^{\frac{1}{2}} \quad (3.5b)$$

The wavelength dependence of the absorption coefficient, $\alpha = \alpha(\lambda)$, creates a wavelength dependence of $J_e = J_e(\lambda)$ as well. The numerical values of J_e for different intensity light lines are shown in Fig. 3.2. Data of the intensity lines was taken from an Hg quartz lamp and is given in Appendix D.

The numerical solution of Eq. (1.9b) with boundary value conditions given by Eq. (1.10) is obtained by using a combination of

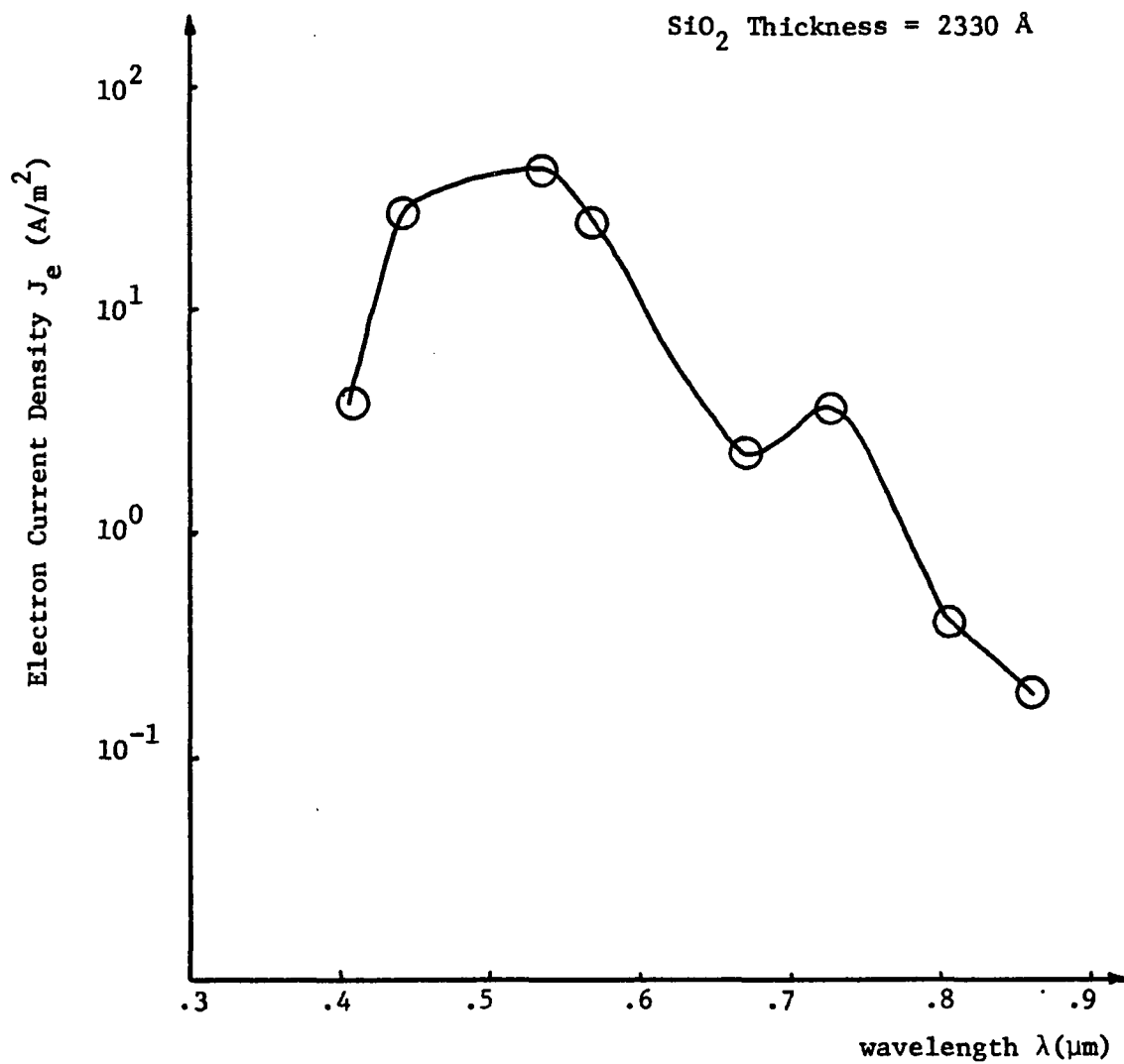


Fig. 3.2 Calculated Electron Current Density Spectral Response for SiO_2 -Si Light Detector

Fourth Order Runge-Kutta-Nystrom and "Shooting" Numerical Methods. Runge-Kutta-Nystrom methods are well adapted for numerical solutions of initial value problems (Kreyszig 1972). "Shooting" methods are adapted for solving boundary value problems by using initial value problems in differential equations (Gerald 1978). The Runge-Kutta-Nystrom numerical solution of the initial value problem

$$y'' = f(x, y, y') \quad (3.6a)$$

$$y(a) = y_a ; y'(a) = y'_a \quad (3.6b)$$

consists of calculating the values

$$A_n = \frac{1}{2} hf(x_n, y_n, y'_n)$$

$$B_n = \frac{1}{2} hf(x_n + \frac{1}{2}h, y_n + \beta_n, y'_n + A_n) \quad (3.7a)$$

$$C_n = \frac{1}{2} hf(x_n + \frac{1}{2}h, y_n + \beta_n, y'_n + B_n)$$

$$D_n = \frac{1}{2} hf(x_n + h, y_n + \delta_n, y'_n + 2C_n) ,$$

where

$$\beta_n = \frac{1}{2}h(y'_n + \frac{1}{2}A_n)$$

$$\delta_n = h(y'_n + C_n) ;$$

(3.7b)

then the new value

$$y_{n+1} = y_n + h(y'_n + K_n) \text{ is used ,} \quad (3.8a)$$

where

$$K_n = (A_n + B_n + C_n)1/3 \quad (3.8b)$$

and

$$y'_{n+1} = y'_n + M_n , \quad (3.9a)$$

with

$$M_n = (A_n + 2B_n + 2C_n + D_n)1/3 \quad (3.9b)$$

and $h = \text{step size of the } x \text{ increment} = \frac{(b - a)}{n}$; $n = \text{integer}$.

The shooting method consists of the following: create an initial value problem, solve it numerically, and compare it with the given conditions at the other boundaries; repeat the solution of this initial value problem with varying values of the assumed conditions until agreement is obtained at the other boundary. For the case of a second order differential equation, the shooting method makes use of the extrapolation formula for slopes

$$\begin{array}{l} \text{Extrapolated estimate} \\ \text{for initial slope} \end{array} = G_1 + \frac{G_2 - G_1}{R_2 - R_1} (D - R_1) \quad (3.11a)$$

where

$G_1 = \text{first guess at initial slope}$

$G_2 = \text{second guess at initial slope}$

$R_1 = \text{first result at end point (using } G_1)$

$R_2 = \text{second result at end point (using } G_2)$.

(3.11b)

Fig. 3.3 shows a flow diagram of the numerical method employed.

A plot of the results of a numerical solution to Eq. (1.9b) is shown in Fig. 3.4. This plot shows the spectral response of the current density of the holes across the field induced junction. The spectral response of the total current density, $J_T = J_e + J_p$, across the

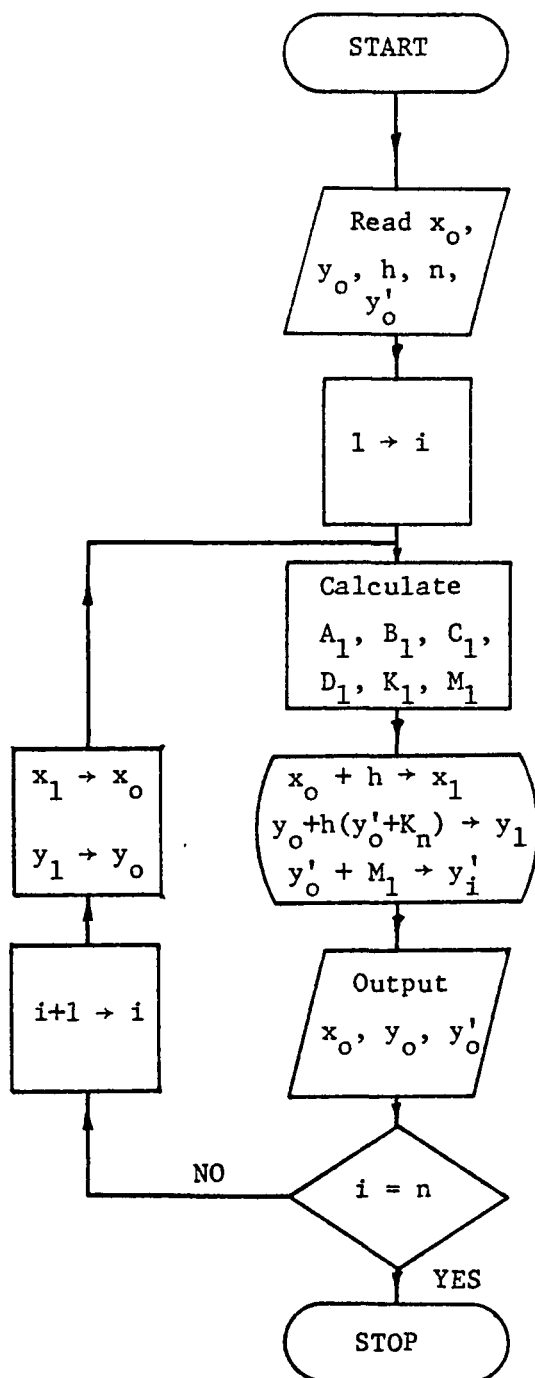


Fig. 3.3 Flow diagram for a Fourth Ordered Runge-Kutta-Nystrom Numerical Analysis

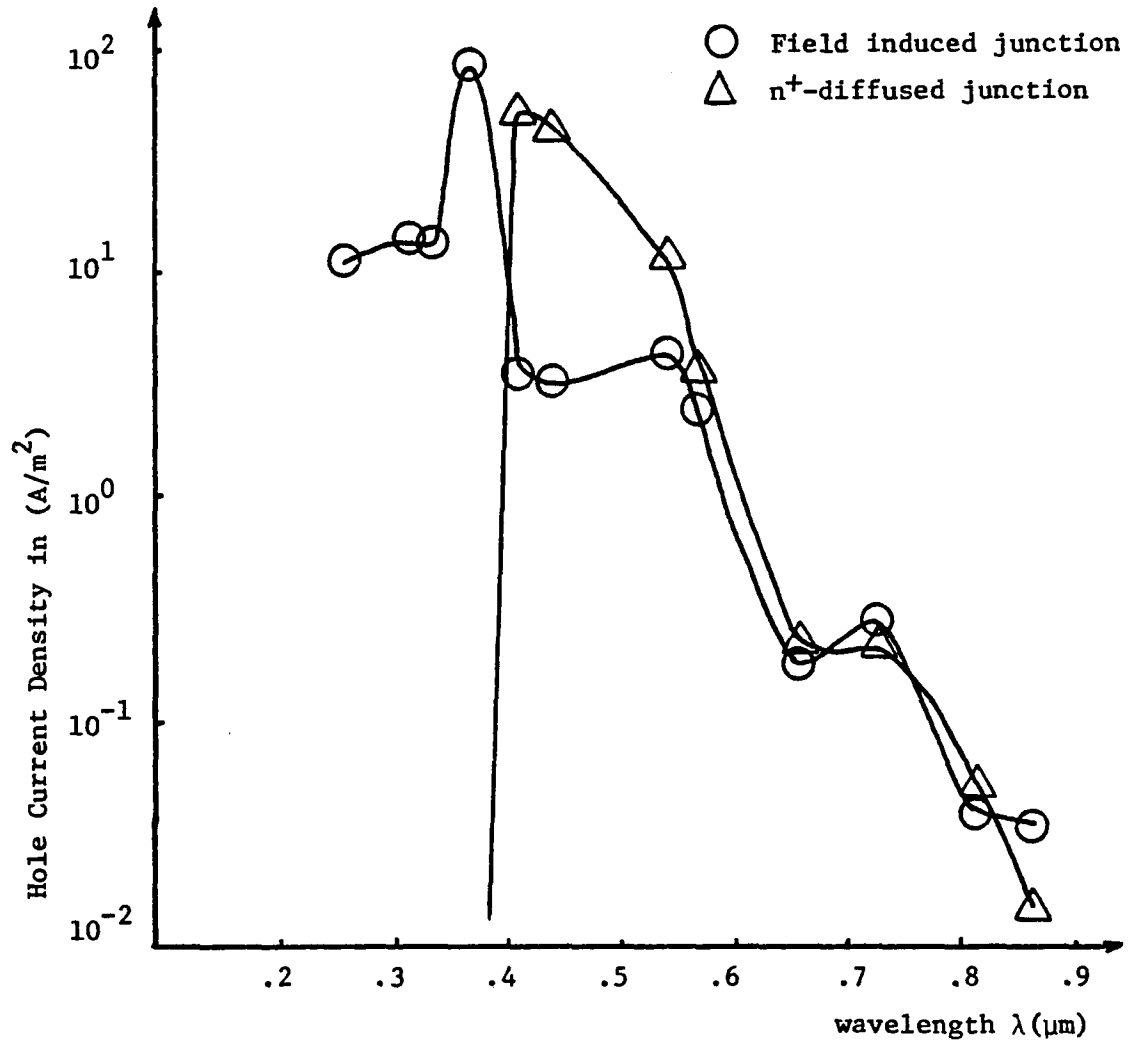


Fig. 3.4 Calculated Hole Current Density Spectral Response of an n^+ -Diffused Junction Detector and a Field Induced Detector

SiO₂-Si light detector is shown in Fig. 3.5. Under these conditions it is possible to obtain the quantum efficiency of the device by means of Eq. (1.1). The spectral dependence of this efficiency is shown in Fig. 3.6.

Discussion

The spectral response of the current density of electrons in the p-region of the device (base), as seen from Fig. 3.2, shows that J_e decreases considerably in regions close and below 0.4 μm . This decrease is produced mainly by the large increases in the values of α in this region of the spectrum. The $\exp(-\alpha x_j)$ factor in Eq. (3.5a) makes J_e depend on α in an exponential manner for these large values. On the other hand, for regions of wavelength around 0.4 μm its spectral response is mainly dominated by the factor

$$\frac{q\phi_0(1-R)\alpha L_e}{(\alpha^2 L_e^2 - 1)},$$

which appears in Eq. (3.5a) and whose value increase as α approaches the value L_e^{-1} .

The calculated spectral response of the current density of holes in the field induced n-region, as seen from Fig. 3.4, shows a sensitive increase in the region between 0.4 μm and 0.25 μm . These numerical calculations assume that the value of the surface recombination velocity $S_p \approx 2.5 \times 10^3$ m/sec. The high value of S_p does not have a considerable detrimental effect on the spectral response of the cell in the range between 0.4-0.25 μm as it does in the impurity diffused

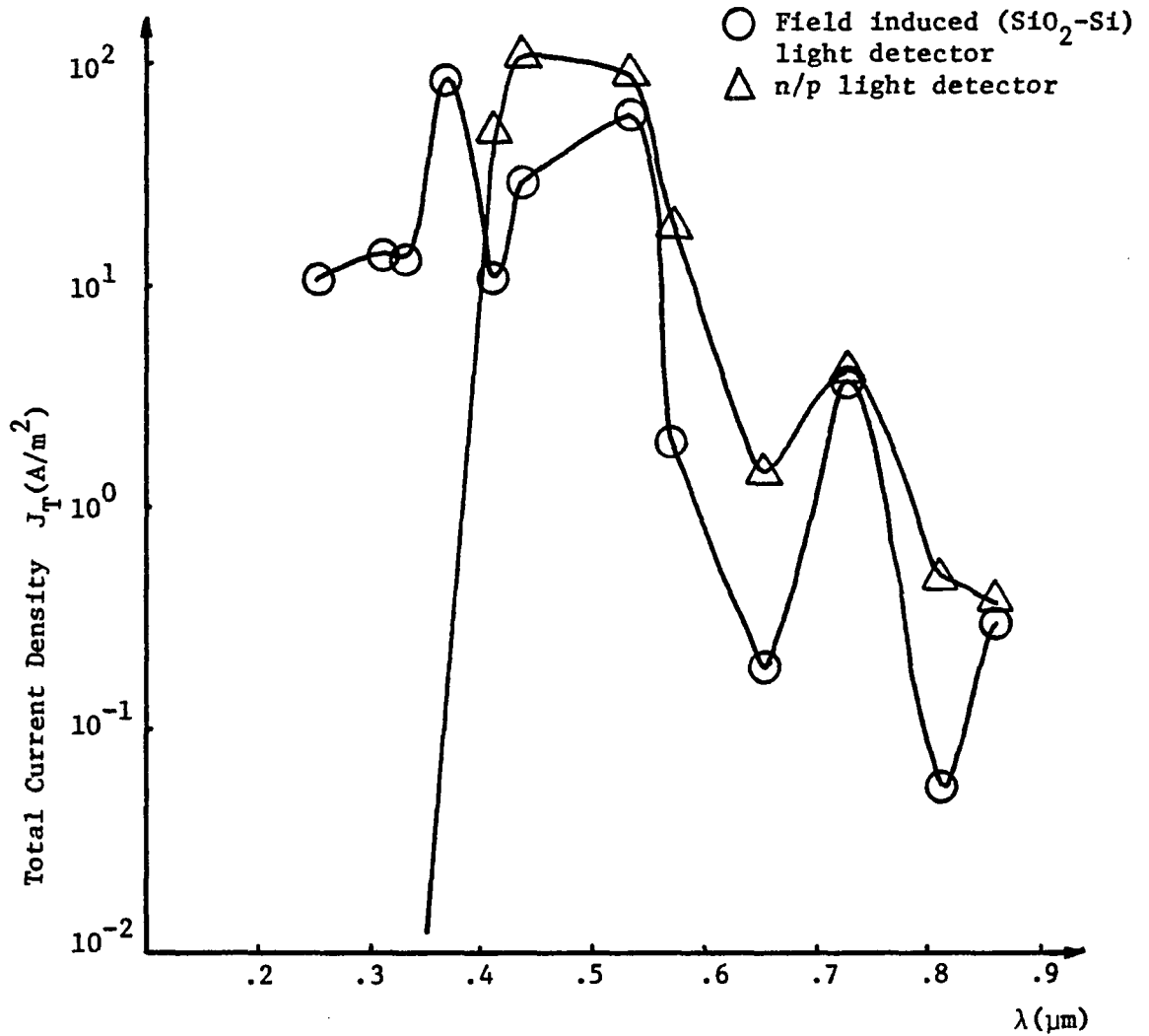


Fig. 3.5 Total Current Density Spectral Response Comparison between an n/p Diffused and a Field Induced $\text{SiO}_2\text{-Si}$ Light Detector

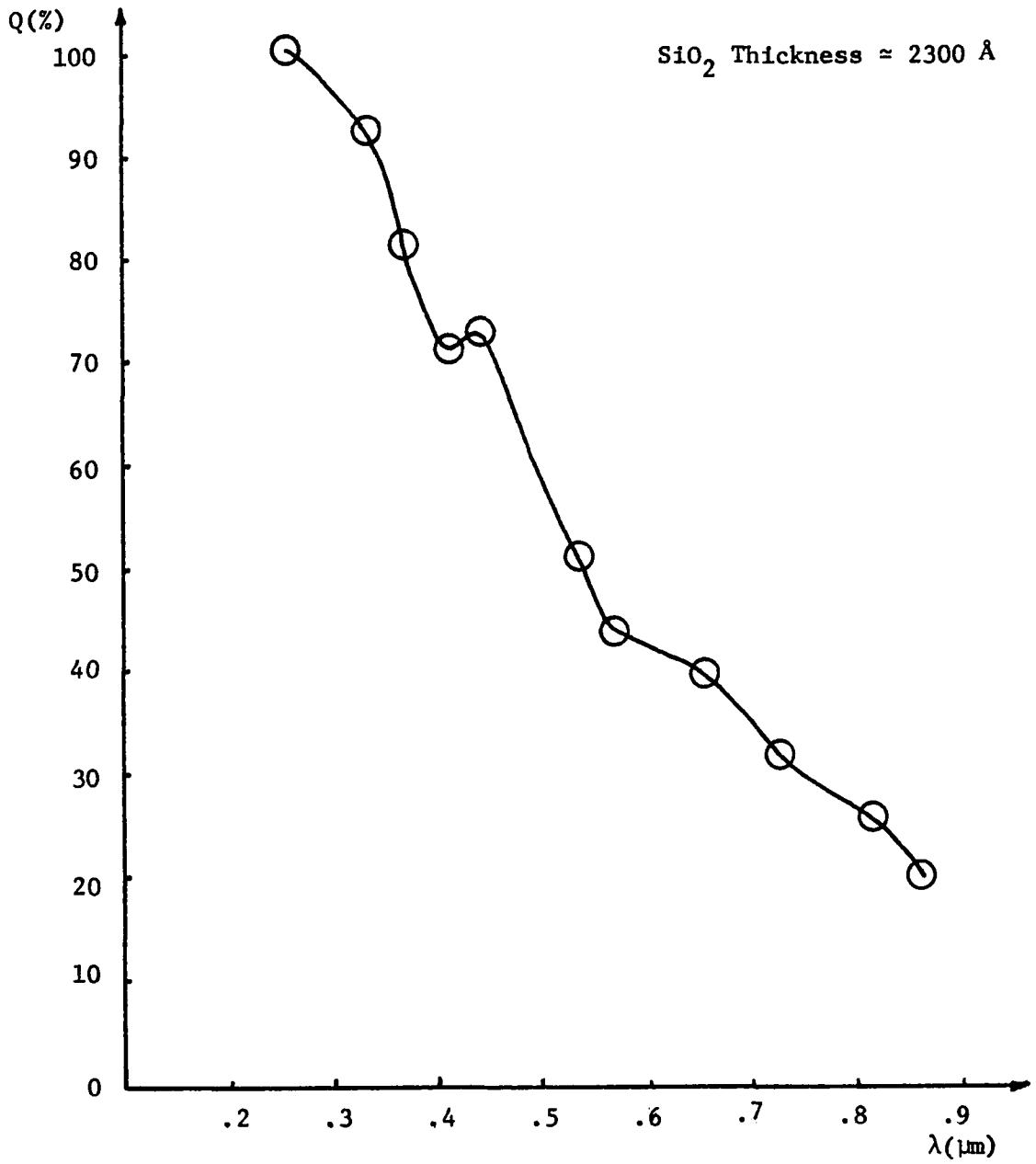


Fig. 3.6 Calculated Quantum Efficiency of the SiO_2 -Si Light Detector

light detectors. This enhanced ultraviolet-visible response is due mainly to the high value of the electric field across the induced junction; its value is maximum at the surface of the light detector where most of the light generated electron-hole pairs are produced by the most energetic photons falling onto the active area of the device. This situation is just the opposite to that in the impurity diffused detectors where the "built in" electric field attains its maximum value just below the surface of the device at the metallurgical junction. As a comparison in the spectral response between the field induced and impurity diffused light detector, Fig. 3.4 shows the current density J_h spectral response of both detectors. In Fig. 3.5 is shown the spectral response of the total current density in the SiO_2 -Si light detector. This figure shows an enhancement in the ultraviolet light response of the detector; in the visible region, the response of the induced junction detector is similar to that of an impurity diffusion detector. For comparison Fig. 3.5 also shows the total spectral response of an impurity diffused light detector. The spectral response of the current density in an impurity diffused light detector is found a way similar to that of the field induced detector, with the sole exception in this case, that the spatial dependence of the electric field in Eq. (1.9b) is neglected.

Summary

A numerical analysis method for the solution of the one dimensional boundary value problem, given by Eqs. (1.9b) and (1.11), was

employed to find the quantum efficiency of the anodic SiO_2 -Si light detector. A numerical solution was found using the "depletion approximation" for the electric field. This approximation assumes a linear spatial dependence of the electric field; the value of this electric field is maximum at the SiO_2 -Si interface and its value depends on the density of surface charge on the Si surface. Typical experimental data of surface charge generation given in Chapter 2 was used in these numerical calculations. The current density spectral response as well as the quantum efficiency of the device, based on the Runge-Kutta-Nystrom numerical analysis, show an enhancement in the response of the detector in the range between $0.4 \mu\text{m}$ and $0.25 \mu\text{m}$ relative to an impurity diffused light detector; this contribution is mainly generated by the field induced p-n junction at the interface of an anodic SiO_2 -Si light detector.

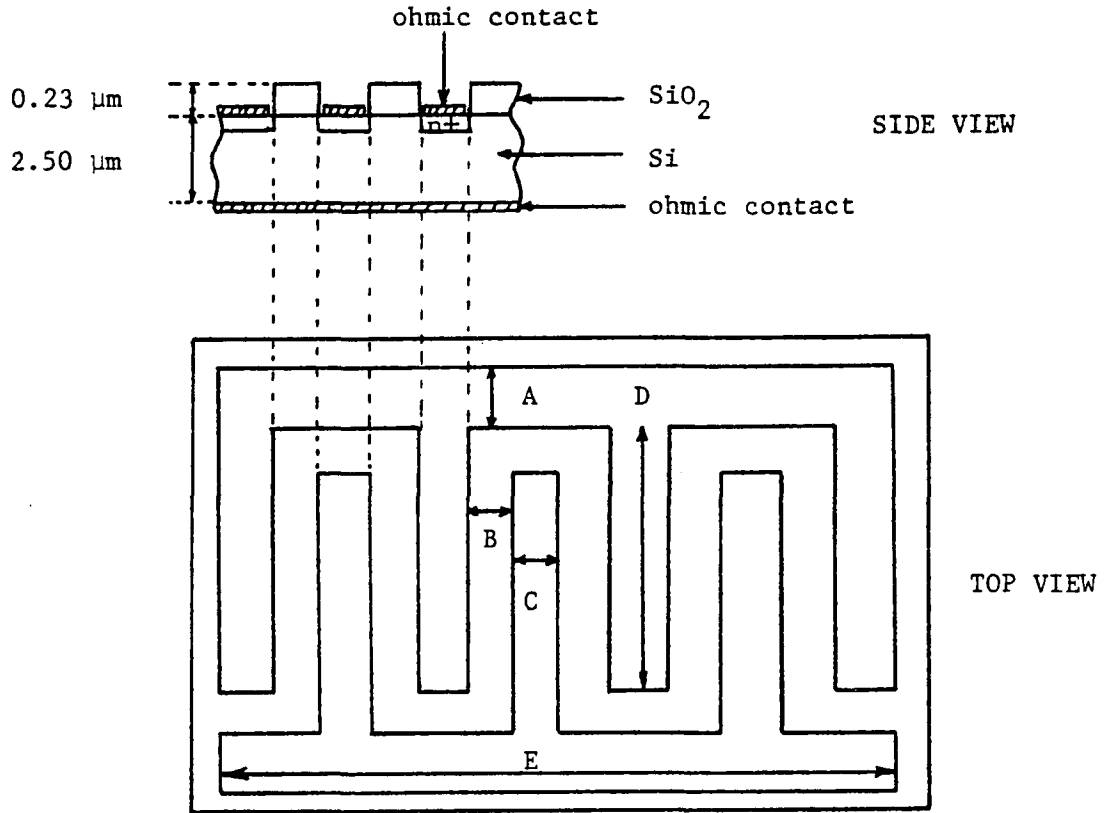
CHAPTER 4

FABRICATION OF THE ANODIC SiO_2 -Si LIGHT DETECTOR

This chapter presents the methods and technologies employed for the fabrication of an anodic SiO_2 -Si light detector. It also discusses the experimental methods used for testing the current density spectral response and the quantum efficiency of the device.

Geometrical Arrangement of the Device

The SiO_2 -Si light detector was fabricated in The University of Arizona Solid State Laboratory. Its active area consists of an interface surface region between an anodically grown SiO_2 layer and a single crystal silicon material. Provisions for collecting the light generated charge carriers in the field induced n-region are made by opening elongated ohmic contact windows in the anodic SiO_2 layer; also, charge carrier collection in the p-region of the detector is made by a direct ohmic contact to the back of the silicon material. Fig. 4.1 shows the geometrical arrangement of the SiO_2 -Si light detector. The average distance between finger contacts is about $366 \mu\text{m}$, the length of the finger contacts is about $1.37 \times 10^{-2} \text{ m}$ and its width is $102 \mu\text{m}$. The total area of the silicon wafer in which the anodic SiO_2 -Si light detector was fabricated is $4 \times 10^{-4} \text{ m}^2$; the area of the detector is $2.28 \times 10^{-4} \text{ m}^2$, and the active area of the device is $2.03 \times 10^{-4} \text{ m}^2$.



Dimensions: A = 478 μm
 B = 366 μm
 C = 102 μm
 D = 1.37×10^4 μm
 E = 1.52×10^4 μm
 $A_T = 2.03 \times 10^{-4}$ m^2

Fig. 4.1 Geometrical Arrangement of the Anodic SiO₂-Si Light Detector

Note: Dimensions are not to scale

Materials Used

In the fabrication of the SiO_2 -Si light detector, .02 by .02 m p-type single crystal wafers, with crystal orientation $\langle 111 \rangle$, and with value resistivities between .10 to 0.15 ohms x m were used. Aluminum evaporated pellets 99.9% pure were used for the front and back ohmic contacts of the SiO_2 -Si diodes. The ion implantation gaseous source used for the n^+ ohmic contact regions was phosphorus trifluoride (PF_3).

Fabrication Procedures

The procedures for the fabrication of anodic SiO_2 -Si light detector consist mainly of three important steps: the Anodic Oxide Growth, the Ion Implantation of Phosphorus for the n^+ ohmic contacts, and the Metal Evaporation for the ohmic contacts. The details of preparation of the Si wafers for each one of these steps are given in Appendices F through H.

Anodic Oxide Growth Assumptions

For purposes of fabrication of anodic SiO_2 -Si light detectors, a molar concentration of KNO_3 salts of 0.04 M was selected in the process. This molarity will ensure that the Q_{ss} generation, after the anodization of Si wafers, will be enough to invert the Si surface at the SiO_2 -Si interface. The electrolyte used for each wafer was freshly made; four Si wafers were selected for anodic oxidation with growth conditions given in Table 4.1.

Table 4.1. Anodic Oxidation Growth Conditions for Batch I

Wafer Number	Anodic Current	Forming Voltage
I-1	25 mA	400 v
I-2	50 mA	400 v
I-3	25 mA	400 v
I-4	50 mA	400 v

The above forming voltage will produce SiO_2 layers of approximately 2200-2300 Å.

Ion Implantation of Phosphorus

The n^+ contact regions of the SiO_2 -Si detectors assume a concentration of donor atoms of about 10^{26} m^{-3} at the surface of the Si material. This amount of impurity atoms in the ohmic contact regions can be obtained with a high dose ion implantation of phosphorus atoms $> 10^{21}$ atoms per m^3 . With this high dose of phosphorus atoms, it is possible to activate them electrically by adding an annealing step to the implanted Si wafers at a temperature of about 620°C under an inert atmosphere (Vasil'ev et al. 1968). Calculations of the phosphorus implantation parameters are made in Appendix I. A summary of these calculated parameters is given in Table 4.2.

Under the assumptions of Table 4.2, an n^+ -p junction depth $x_j \approx 0.197 \text{ } \mu\text{m}$ is obtained and a surface concentration of impurity phosphorus atoms of $N_s \approx 10^{26} \text{ m}^{-3}$.

Table 4.2. Calculated Parameters for Phosphorus Ion Implantation in the SiO₂-Si Device.

Parameter	Dose	Energy	Time
Value	1.25x10 ¹⁹ at/m ²	100 Kev	22.7 min

Metallization Procedure

The collection of photo generated carriers in the SiO₂-Si light detector at the n⁺ region is made by using aluminum ohmic contacts. The aluminum evaporation occurs at pressures of 10⁻⁶ torr and a temperature of about 700°C; the aluminum finger pattern is made by standard photolithographic techniques.

Measurement Procedures

The spectral response of a photodiode is defined as the short circuit current as a function of the wavelength of the incident light. The short circuit current of the anodic SiO₂-Si light detector is obtained by connecting the front and back ohmic ocntacts of the device and measure this short circuit current.

Lock-in detection techniques were used for measurement of the spectral response of the anodic SiO₂-Si light detector. This technique allows detection of low electric signals. The lock-in analyzer employed for the electric signal measurements was an ITHACO DYNATRAC 3 Lock-in analyzer model 393-01. The monochromatic light was obtained by means of a III 200 watt Mercury short arc lamp and a Jarrell Ash

scanning monochromator model 82-020 at the Quantum Electronics Laboratory of The University of Arizona. The chopping of the monochromatic light at the exit slit of the monochromator was controlled by means of a direct current (d.c.) motor employing a chopping wheel with two slots. Monitoring of the amount of radiation of light at the exit slit of the monochromator was made by using two photomultipliers with cathode responses S-1 and S-13. Fig. 4.2 shows the experimental arrangement of this method.

Measurements on the dark I-V characteristics of the anodic SiO₂-Si device were made. The results on such measurements are used to calculate the series resistance of the device, R. This series resistance is operationally defined as

$$R = \frac{V_1 - V_0}{I_1} \quad (4.2)$$

where V_1 is measured at sufficiently large current I_1 to cause V_1 to deviate from the ideal forward voltage V_0 by at least 100%. V_0 is obtained by logarithmically extrapolating the diode forward voltage drop at the low diode currents to the current I_1 . Fig. 4.3 shows graphically this method (Hamstra and Wendland 1972).

To account for the series resistance, R_{s2} , originated mainly by the n-inversion region of the SiO₂-Si detector, (active region), a set of measurements were made on the device under light conditions using the method of Handy (R. J. Handy 1967). For such measurements a tungsten light source was employed; provisions were made as to maintain a room temperature in the device during this set of measurements.

Scanning Monochromator

Current to Voltage Converter

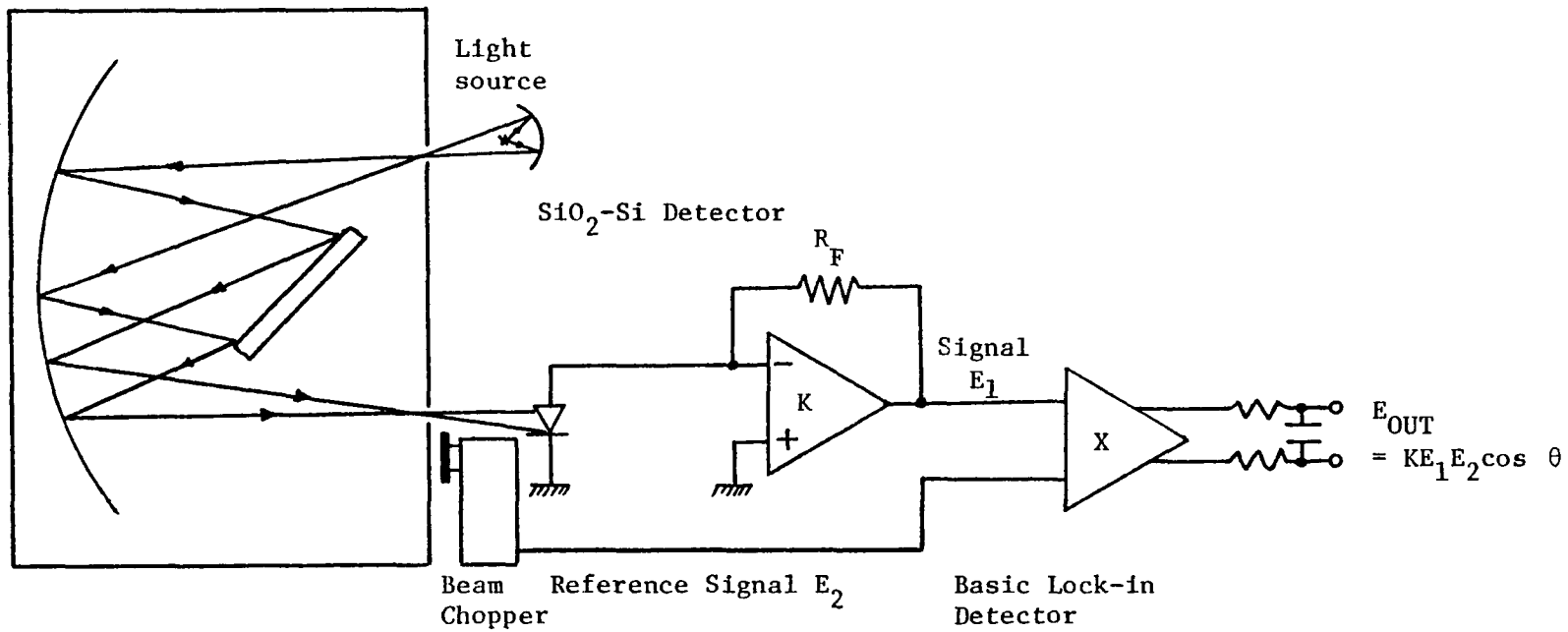


Fig. 4.2 Experimental Arrangement to Measure the Spectral Response of the $\text{SiO}_2\text{-Si}$ Light Detector

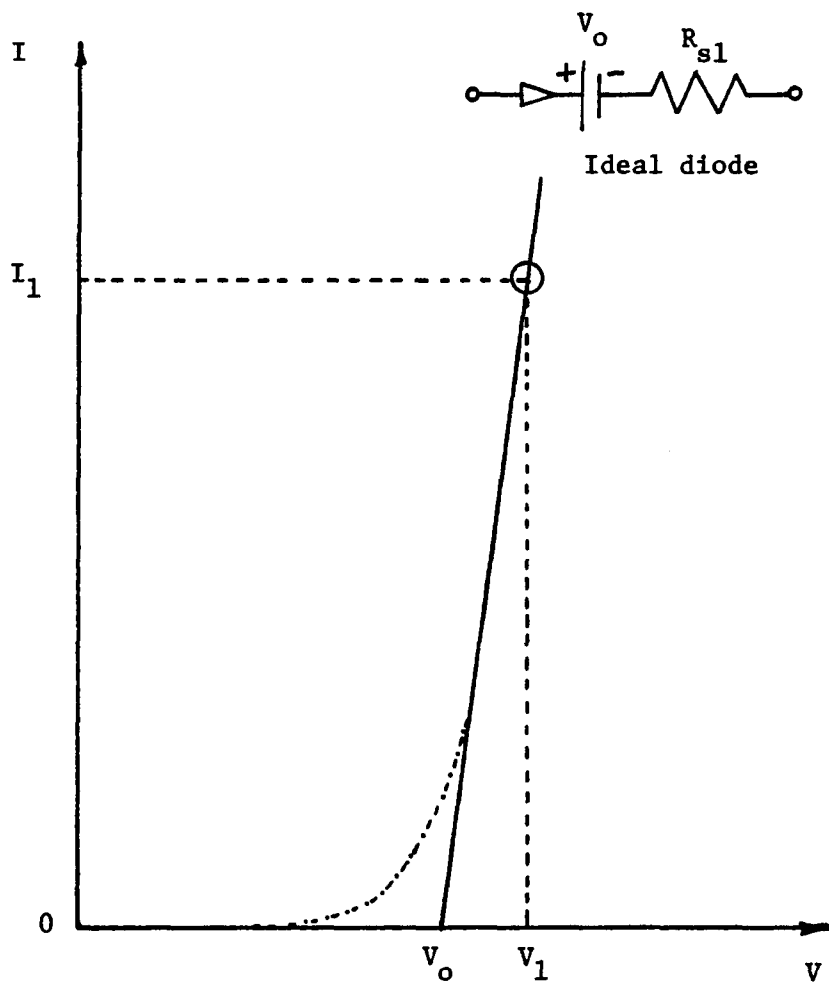


Fig. 4.3 Ideal Diode I-V Curve with Offset Voltage and a Series Resistance

Results

Results in the spectral response of the anodic SiO_2 -Si light detector are shown in Fig. 4.4. This set of values were taken using an effective bandwidth B_{eff} of value $B_{\text{eff}} = 0.1$ hz and a light chopping frequency of 22 hz. Calculations of the quantum efficiency of the device, using the spectral response shown in Fig. 4.4, are shown in Fig. 4.5. For comparison, Fig. 4.5 also includes the theoretical quantum efficiency calculated in Chapter 3.

The calculated values of R and R_{s2} of the dark and light conditions, respectively, are shown in Table 4.3. The I-V characteristics of the anodic SiO_2 -Si light detector under the fluorescent light are shown in Fig. 4.6.

Discussion of Results

The quantum efficiency of the SiO_2 -Si detector, shown in Fig. 4.5, shows two important results. First, the low temperature fabrication process of the device, ($< 620^\circ\text{C}$), has a considerable effect on the improved response of the detector in the wavelength range 0.7 - $0.9 \mu\text{m}$. Second, that the high value of the electric field at the surface of the Si material clearly improves its ultraviolet response in the range 0.2 - $0.4 \mu\text{m}$. The first result is originated by an increased value in the lifetime of the electrons since no high temperature cycles, ($> 620^\circ\text{C}$), are involved; the value of the electron lifetime employed in the calculations of the electron current J_e , Eq. (3.5a) was taken as a representative of the electron lifetime value

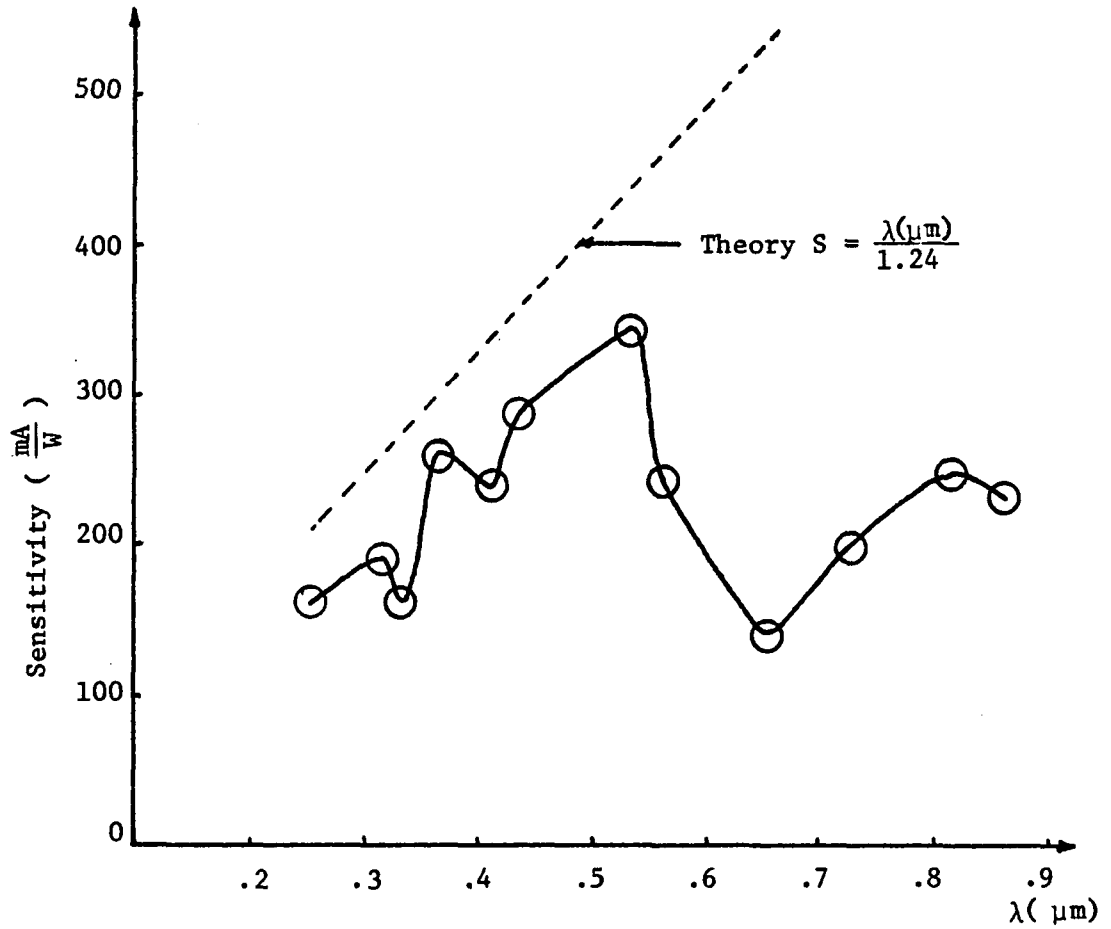


Fig. 4.4 Sensitivity Spectral Response of the Anodic SiO_2 -Si Light Detector

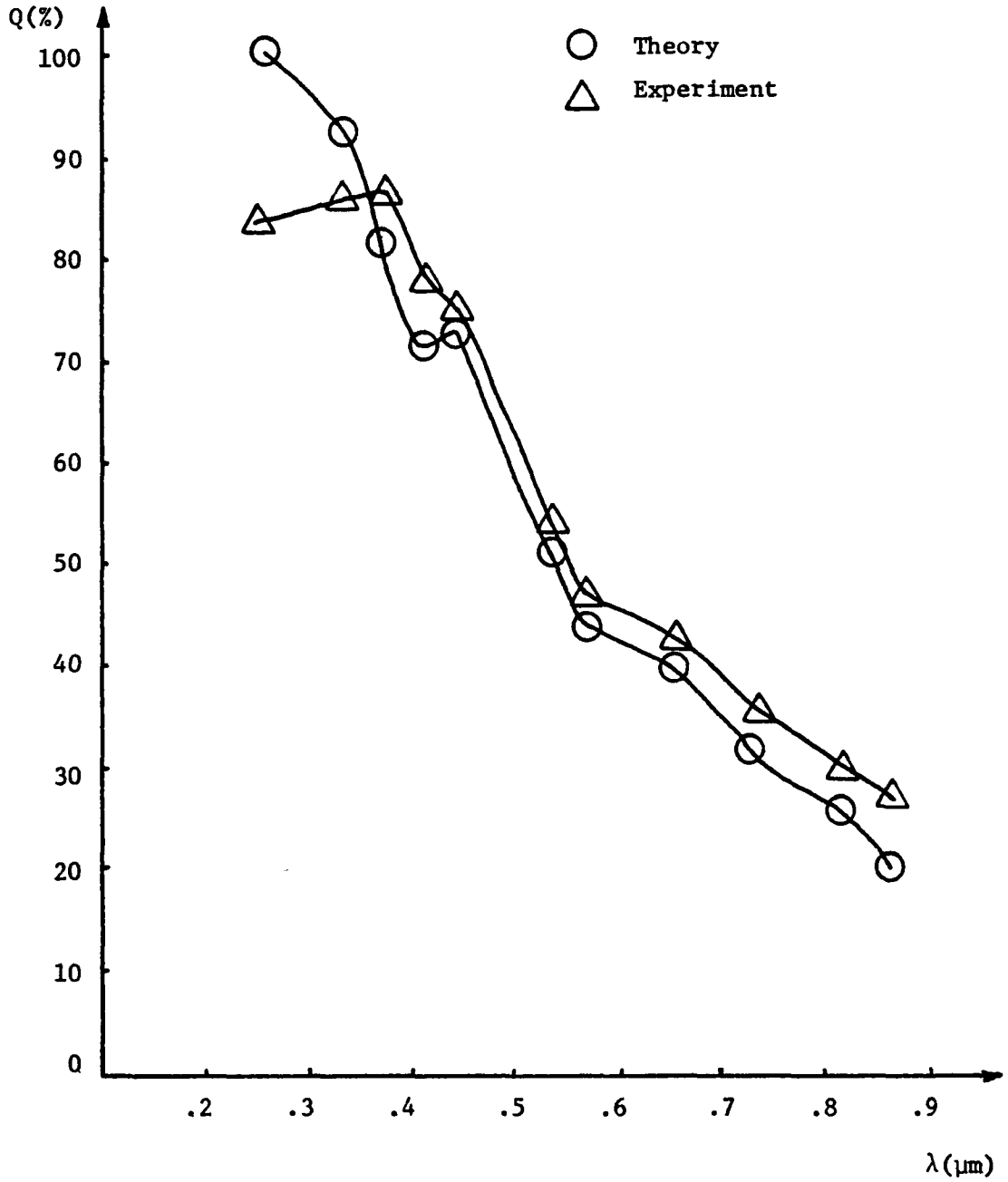
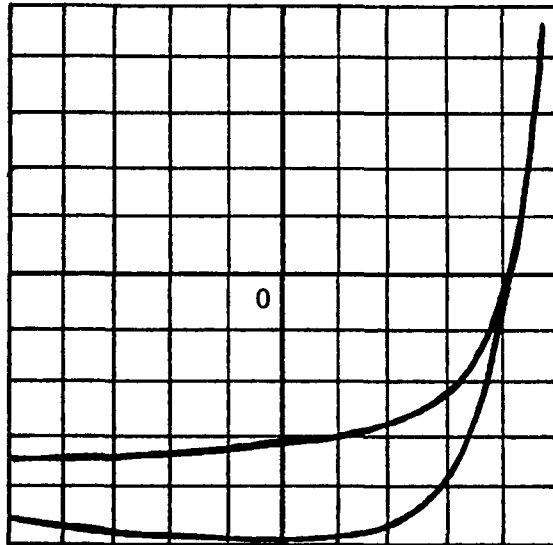


Fig. 4.5 Comparison between Theoretical and Experimental Quantum Efficiencies for the Anodic SiO_2 -Si Light Detector

Table 4.3 Results in the Calculations of R, and R_{s2}

Condition	Dark	With Light
Value	$R \approx 2.30$ ohms	$R_{s2} \approx 7.24$ ohms



Horizontal axis = 0.1 v/div

Vertical axis = 0.2 mA/div

Fig. 4.6 I-V Characteristics of the SiO_2 -Si Light Detector under a Fluorescent Light Lamp

The I-V curves shown here are trace drawings of an oscillogram picture. The lower curve represents the I-V characteristics of the SiO_2 -Si light detector under light conditions. The upper curve shows only a retracing effect of the electron beam in the oscilloscope screen.

for devices subject to high temperature fabrication. The second result is originated by the spatial dependence of the electric field which causes the free holes in the n inversion region to cross it in an average time given by

$$t = - \frac{x_M}{E_M \mu_p} \log \left(1 - \frac{x_i}{x_M} \right) \approx 5.58 \times 10^{-12} \text{ sec} \quad (4.3)$$

This "traveling time" of holes in the inversion region, assumes that the electric field at the surface of the Si material is $E_M \approx 2.5 \times 10^6$ volt/m and $\mu_p \approx 2.5 \times 10^{-2} \text{ m}^2/\text{volt sec}$. The numerical value of Eq. (4.3) is approximately four orders of magnitude smaller than the lifetime of the holes used in solving Eq. (1.9b); this value will allow most free holes in the n-region to cross it before they recombine there.

The difference in the measured values of R and R_{s2} under different measurement conditions can be explained as follows. Under dark conditions, most of the injected carriers in the front and back ohmic contacts of the device travel across the n^+-p region and the n-p region; injected carriers thus encounter resistive paths in both regions which give the value

$$R = R_{s1} \parallel R_{s2} \quad (4.4)$$

where

R_{s1} = resistance due to n^+-p region

R_{s2} = resistance due to n-p region

Under light conditions, the measured value R_{s2} , is higher than that under dark condition measurements. It is believed that the light

generated carriers cross the n^+ -n-p region and this path is the cause for the value R_{s2} . The n^+ -p region under light conditions does not contribute to light generated carriers because light cannot reach the n^+ region due to the aluminum contact layer on top of this ion implanted region.

Summary

The spectral response of the anodic SiO_2 -Si light detector was measured. To measure this response, the short circuit current of the device was measured using lock-in detection techniques. The light source employed in these measurements was a high pressure mercury lamp. The results show an increase in the ultraviolet response, 0.2-0.4 μm , of the device due to the presence of a high electric field across the interface anodic SiO_2 -Si. These measurements also show an improved response of the detector in the range 0.7-0.9 μm as compared with the predicted theoretical spectral response; this increased response of the device is originated because of the low temperature, ($< 620^\circ\text{C}$), fabrication of the light detector. This method of fabrication enhances the lifetime of the electrons in the p-region.

Two methods of measurement on the series resistance of the device were made. The first method gives the result of the series resistance, R , due to the contribution of the two regions, n^+ -p and n-p. The second method gives the result of the resistance, R_{s2} , due to the contribution of the region n^+ -n-p. The two values of the series

resistance obtained by these two methods are different, indicating that there are two different electric paths of the carriers under these two conditions of measurement.

CHAPTER 5

SUMMARY AND CONCLUSIONS

The general objective of this dissertation was to fabricate and test a new ultraviolet-visible light detector: The anodic SiO_2 -Si light detector. This device was expected to function with the help of surface state charges Q_{ss} generated at the interface of a low temperature grown anodic SiO_2 and an Si single crystal material.

Previous work on the fabrication of inversion light detectors requires high temperature fabrication cycles which could have detrimental effects on the lifetime of minority carriers in the material used,

Summary

A general discussion was presented of the problems encountered in the fabrication of a light detector sensitive to the ultraviolet range 0.2-0.4 μm . It was suggested that the low temperature fabrication of the SiO_2 -Si light detector could alleviate some of the problems. Mention was also made of the objectives that this dissertation would pursue by the study and fabrication of anodic SiO_2 -Si light detectors. A mathematical method for the continuity equation of the free charge carriers in the SiO_2 -Si device was made. This model showed that the spatial dependence of the electric field in the n-inversion region,

generated by surface state charges Q_{ss} , would require the mathematical equation to be treated numerically.

An experimental study was made to optimize the surface state charge generation at the anodic SiO_2 -Si interface. It was found that the surface charge increased as the molar concentration of KNO_3 salts increased in the electrolyte used in the anodic oxidation of silicon. There was a limit in this surface charge generation however. Molarities greater than 0.08 M produced contaminated SiO_2 layers. Another finding was that this surface charge generation is a function of the amount of current density in the anodization cell. There exist a limit on the charge generation. This limit is set by the production of porous SiO_2 -Si layers.

A simplified model of the electric field and electrostatic potential through the n-inversion region was employed. This model, sometimes called the "depletion approximation" was used to find a numerical solution of the continuity equation for holes in this inversion layer region. The numerical values of this solution were taken to calculate the quantum efficiency of the SiO_2 -Si detector. Some of the parameters used in this numerical solution, such as the electrostatic potential value at the surface of the silicon material, were borrowed from the experimental findings on surface state charge generation. The quantum efficiency of the device thus calculated, showed that SiO_2 -Si light detector has an enhanced response in the range 0.25-0.4 μm of the spectrum.

Finally, using the anodic oxide growth techniques employed in the experiments on surface state charge generation, an anodic SiO_2 -Si light detector was fabricated. The spectral response of this device was measured employing lock-in detection techniques. The results of such measurements show that this device has an enhanced ultraviolet light response (0.25-0.4 μm), and an improved light response in the range 0.7-0.9 μm . The electric field at the interface of the SiO_2 -Si system and the low temperature fabrication ($< 620^\circ\text{C}$) of this device account for such findings.

Recommendations for Future Work

Anodic SiO_2 -Si light detectors provide an interesting source for future work in the area of solar energy converters. This area of work requires that these devices be fabricated with the least expense of energy. The low temperature fabrication of the anodic SiO_2 -Si light detector has this feature. The ion implantation technique employed in the fabrication of this type of device however, requires the availability of expensive ion implantation facilities. MIS cells on the other hand, using anodic SiO_2 could be investigated as an alternative to the ion implantation n^+ regions. Studies on the interface surface state charge generation between anodic SiO_2 and polycrystalline silicon materials could offer alternative ways to produce solar energy converters by means of low temperature fabrication.

APPENDIX A

PROCEDURE FOR Si WAFER CLEANING

1. Clean wafers' surface with a Q tip and acetone and blow dry with N_2 .
2. Immerse wafers in a 3:1 sulfuric acid: hydrogen peroxide mixture at $T = 100^\circ C$ and $t = 6$ minutes.
3. Rinse wafers in DI water (> 2 megohms of resistivity) for $t = 5$ minutes.
4. Blow wafers dry with N_2 and immerse them in a 10:1 H_2O (DI):HF (46%) solution for $t = 1$ min.
5. Rinse wafers in DI water ($R > 2$ megohms) and blow them dry with N_2 .
6. Immerse wafers in Nitric acid at $T = 90^\circ C$ for $t = 6$ minutes.
7. Rinse wafers in DI water for 5 minutes.
8. Blow wafers dry with nitrogen and protect them from dust.

APPENDIX B

PREPARATION OF MOLAR SOLUTIONS

To prepare molar solutions of potassium nitrate (KNO_3) in ethylene glycol ($\text{C}_2\text{H}_6\text{O}_2$) follow the steps below:

1. Select appropriate molarity.
2. Mix amount of KNO_3 salt and ethylene glycol in a glass container (sealed).
3. Immerse glass container with solution in an ultrasonic bath for $t = 2$ hrs. or until salt is completely dissolved.

APPENDIX C

SiO₂ GROWTH CHARACTERISTICS OF WAFERS

Notation: dx/dt = oxide thickness/unit time

dV/dt = forming voltage/unit time

Wafer Number	dx/dt (m/sec)	dV/dt (volt/sec)	E field (volt/m)	Q _{ss} /q (m ⁻²)
1	8 x10 ⁻¹¹	0.13	1.63x10 ⁹	1.41x10 ¹⁶
2	2.07x10 ⁻¹⁰	0.24	1.16x10 ⁹	5.51x10 ¹⁵
3	5.40x10 ⁻¹¹	0.24	4.44x10 ⁹	---
4	6.62x10 ⁻¹¹	0.13	1.96x10 ⁹	7.93x10 ¹⁵
5	1.88x10 ⁻¹⁰	0.24	1.28x10 ⁹	3.13x10 ¹⁵
6	5.42x10 ⁻¹¹	0.13	2.40x10 ⁹	8.01x10 ¹⁵
7	6.10x10 ⁻¹¹	0.13	2.13x10 ⁹	9.91x10 ¹⁵
8	1.58x10 ⁻¹⁰	0.24	1.51x10 ⁹	4.11x10 ¹⁵
9	1.88x10 ⁻¹⁰	0.24	1.28x10 ⁹	6.70x10 ¹⁵
10	1.92x10 ⁻¹⁰	0.24	1.25x10 ⁹	7.85x10 ¹⁵
11	6.35x10 ⁻¹¹	0.13	2.05x10 ⁹	5.39x10 ¹⁵
12	1.49x10 ⁻¹⁰	0.24	1.61x10 ⁹	4.19x10 ¹⁵
13	6.07x10 ⁻¹¹	0.13	2.14x10 ⁹	3.91x10 ¹⁵
14	6.60x10 ⁻¹¹	0.14	2.12x10 ⁹	1.75x10 ¹⁶
15	2.07x10 ⁻¹⁰	0.24	1.16x10 ⁹	1.78x10 ¹⁶

Wafer Number	dx/dt (m/sec)	dV/dt (volt/sec)	E field (volt/m)	Q_{ss}/q (m^{-2})
17	2.73×10^{-10}	0.24	8.79×10^8	1.68×10^{16}
19	2.6×10^{-10}	0.24	9.23×10^8	2.01×10^{16}
20	1.02×10^{-10}	0.13	1.27×10^9	1.78×10^{16}
21	1.77×10^{-10}	0.24	1.36×10^9	1.73×10^{16}
22	7.3×10^{-11}	0.13	1.78×10^9	9.59×10^{15}
23	3.43×10^{-10}	0.24	7×10^8	1.16×10^{16}
24	7.47×10^{-11}	0.13	1.74×10^9	9.7×10^{15}
25	1.98×10^{-10}	0.24	1.21×10^9	2.04×10^{16}
26	1.49×10^{-10}	0.24	1.61×10^9	1.7×10^{16}
27	8.12×10^{-11}	0.13	1.6×10^9	1.8×10^{16}
28	1.62×10^{-10}	0.24	1.48×10^9	2×10^{16}
30	7.5×10^{-11}	0.13	1.73×10^9	1.86×10^{16}
34	6.22×10^{-11}	0.13	2.09×10^9	1.69×10^{16}
35	5.85×10^{-10}	0.13	1.33×10^9	1.59×10^{16}
36	1.41×10^{-10}	0.24	1.70×10^9	1.58×10^{16}

APPENDIX D

RELATIVE INTENSITY LINES FOR AN Hg LAMP

Hg Lamp type III-203

Line (Å)	2537	3050	3150	3650	4050	4350
Rel. Int.	0.12	5.20	6.80	12.9	7.90	9.50
Line (Å)	5450	5750	6683	7301	8097	8703
Rel. Int.	6.70	5.60	0.98	0.54	0.43	0.35

APPENDIX E

LISTING OF A NUMERICAL SOLUTION PROGRAM

The numerical solution program of a differential equation of the type $y'' = f(x,y,y')$ using a Runge-Kutta-Nystrom method is listed below. This program is adapted to a programmable hand calculator Texas Instrument Model TI59.

000	47	CMS		021	42	STD
001	61	GTO		022	05	05
002	02	02		023	76	LBL
003	57	57		024	43	RCL
004	76	LBL		025	71	SBR
005	11	A = x_0		026	48	EXC
006	42	STD		027	53	(
007	01	01		028	93	.
008	91	R/S		029	05	5
009	76	LBL		030	65	*
010	12	B = y_0		031	43	RCL
011	42	STD		032	05	05
012	03	03		033	65	*
013	91	R/S		034	71	SBR
014	76	LBL		035	44	SUM
015	13	C = y'_0		036	54)
016	42	STD		037	42	STD
017	04	04		038	06	06
018	91	R/S		039	53	(
019	76	LBL		040	93	.
020	14	D = h				

041	05	5	081	05	5	121	53	(
042	65	*	082	65	*	122	43	RCL
043	43	RCL	083	71	SBR	123	05	05
044	05	05	084	44	SUM	124	65	*
045	65	*	085	54)	125	53	(
046	53	(086	42	STD	126	43	RCL
047	43	RCL	087	08	08	127	17	17
048	04	04	088	71	SBR	128	85	+
049	85	+	089	48	EXC	129	43	RCL
050	93	.	090	53	(130	09	09
051	05	5	091	93	.	131	54)
052	65	*	092	05	5	132	54)
053	43	RCL	093	65	*	133	42	STD
054	06	06	094	43	RCL	134	10	10
055	54)	095	05	05	135	71	SBR
056	54)	096	54)	136	48	EXC
057	42	STD	097	44	SUM	137	43	RCL
058	07	07	098	16	16	138	05	05
059	53	(099	43	RCL	139	44	SUM
060	93	.	100	07	07	140	16	16
061	05	5	101	44	SUM	141	43	RCL
062	65	*	102	17	17	142	10	10
063	43	RCL	103	43	RCL	143	44	SUM
064	05	05	104	08	08	144	17	17
065	54)	105	44	SUM	145	53	(
066	44	SUM	106	18	18	146	02	2
067	16	16	107	53	(147	65	*
068	43	RCL	108	93	.	148	43	RCL
069	07	07	109	05	5	149	09	09
070	44	SUM	110	65	*	150	54)
071	17	17	111	43	RCL	151	44	SUM
072	43	RCL	112	05	05	152	18	18
073	06	06	113	65	*	153	53	(
074	44	SUM	114	71	SBR	154	93	.
075	18	18	115	44	SUM	155	05	5
076	53	(116	54)	156	65	*
077	93	.	117	42	STD	157	43	RCL
078	05	5	118	09	09	158	05	05
079	65	*	119	71	SBR	159	65	*
080	43	RCL	120	48	EXC	160	71	SBR
						161	44	SUM

APPENDIX F

ANODIC OXIDATION OF SILICON WAFERS

1. Prepare a fresh KNO_3 -ethylene glycol electrolyte as explained in Appendix B.
2. Clean the Si wafers as explained in Appendix A.
3. Immediately after cleaning the Si wafers, grow an SiO_2 layer on the Si wafers using the apparatus shown in Fig. 2.4.
4. After SiO_2 growth, clean the Si wafers with Dionized (DI) water and blow them dry with N_2 .

APPENDIX G

PHOSPHORUS ION IMPLANTATION PROCEDURE

1. Grow anodic SiO_2 layers $> 2000 \text{ \AA}$ in ethylene glycol solution as described in Appendix F.
2. Deposit a layer of Photo-Resist (Kodak 747) with spinner at 2500 r.p.m. for $t = 15 \text{ sec.}$
3. Open windows for Phosphorus ion implantation on the Si wafers using standard photolithographic techniques.
4. Etch away the exposed SiO_2 layer in a 10:1 solution of $\text{H}_2\text{O}:\text{HF}$ for $t \approx 20 \text{ sec}$ or until windows look purple (900 \AA).
5. Rinse wafers in DI water and blow them dry with N_2 . Wafers are now ready for phosphorus ion implantation.
6. Do phosphorus ion implantation according to the instructions of the ion implantation machine.
7. After phosphorus ion implantation, strip off the Photo-Resist layer with Kodak J-100 at a temperature of 90°C for $t = 10 \text{ min.}$
8. To anneal Si wafers after phosphorus ion implantation load the Si wafers in a furnace quartz tube at $T = 600^\circ\text{C}$ for $t = 10 \text{ min.}$ under N_2 atmosphere.

APPENDIX H

ALUMINUM EVAPORATION PROCEDURE

1. Rinse the Si wafers with DI water and blow them dry with N₂.
2. Load wafers in the vacuum station and pump pressure down to 10^{-6} torr.
3. Evaporate the aluminum pellets until a deposited aluminum layer is > 5000 Å.
4. If Al sintering is needed on the wafers, load the Si wafers in a furnace quartz tube for $t = 3$ min. at a temperature $T = 450^{\circ}\text{C}$ under mixed atmosphere of 90% of N₂ and 10% of H₂.

APPENDIX I

PARAMETER CALCULATIONS FOR PHOSPHORUS

ION IMPLANT

The impurity profile of Phosphorus ion implant has the form

$$N(x) = \frac{Q/A}{2\pi^{1/2}\Delta R_p} \exp \left\{ - \frac{(x - R_p)^2}{\Delta R_p^2} \right\}$$

where

$N(x)$ = Phosphorus ion concentration

R_p = projected range of implanted ions

ΔR_p = projected standard deviation of implanted ions.

Q/A = total number of ion implanted atoms per unit area (dose).

For an SiO_2 and Si system, the following parameters were selected

Implant energy = 100 Kev

$R_p(\text{SiO}_2) \approx 989 \text{ \AA}$

$R_p(\text{Si}) \approx 354 \text{ \AA}$

$N_{BC} \approx 1.5 \times 10^{21} \text{ m}^{-3}$ (0.1 Ohms x m Si p-type material)

$N_s = N(0) \approx 10^{26} \text{ m}^{-3}$

Using the above data, the following parameters can be calculated:

$$Q/A = 2\sqrt{\pi}N_s R \approx 1.25 \times 10^{19} \text{ m}^{-2}$$

$$x_j \approx \frac{\Delta R}{2} \ln(N_s/N_{BC}) \approx 0.197 \text{ } \mu\text{m}.$$

and for a Gaussian profile

$$\bar{\sigma} \approx 3.5 \times 10^4 \text{ (ohms x m)}^{-1}$$

this gives

$$\rho'_s \approx 145 \text{ ohms/sq.}$$

For the ion implantation machine of the Solid State Laboratory of The University of Arizona

$$3.25 \times 10^{-6} \text{ coul} = 10^{16} \text{ atm/m}^2$$

So for a dose of $Q/A \approx 1.25 \times 10^{19} \text{ m}^{-2}$, 4080 μcoul are needed. From this last value, the total ion implant time is $t \approx 22.7 \text{ min.}$

LIST OF REFERENCES

- Brown, W. L. "N-type Surface Conductivity on P-type Germanium," Physical Review, Vol. 91, No. 3, August 1, 1953.
- Call, R. L. "Inversion Layer Solar Cell Fabrication and Evaluation," Final Report J. P. L. Contract No. 953461, September 1973.
- Chappell, Alan Ed. Optoelectronics: Theory and Practice, Texas Instruments Ltd., 1976.
- Deal, B. E., Sklar, M., Grove, A. S., and Snow, E. H. "Characteristics of the Surface-State Charge (Q_{SS}) of Thermally Oxidized Silicon," J. Electrochemical Society, Vol. 114, No. 3, 1967.
- Gerald, Curtis, F. Applied Numerical Analysis, 2nd Ed., Addison Wesley, 1978.
- Grove, A. S. Physics and Technology of Semiconductor Devices, John Wiley, 1967.
- Grove, A. S., Deal, B. E., Snow, E. H., and Sah, C. T. "Investigation of Thermally Oxidized Silicon Surfaces Using Metal-Oxide-Semiconductor Structures," Solid State Electronics, Vol. 8, 1965.
- Hamstra, Robert H., Jr. and Wendland, Paul, "Noise and Frequency Response of Silicon Photodiode Operational Amplifier Combination," Applied Optics, Vol. 11, July, 1972.
- Handy, R. J. "Thermal Analysis of the Series Resistance of a Solar Cell," Solid State Electronics, Vol. 10, 1967.
- Hovel, Harold, J. Semiconductors and Semimetals, Vol. 11; Solar Cells, Academic Press, 1975.
- Kingston, R. H. and Neustadter, S. F., "Calculation of the Space Charge, Electric Field, and Free Carrier Concentration at the Surface of a Semiconductor," Journal of Applied Physics, Vol. 26, No. 6, June 1955.
- Kreyszig, Erwin. Advanced Engineering Mathematics, 3rd ed., John Wiley, 1972.

- Lindmayer, J. and Allison, J. F. "The Violet Cell: An Improved Silicon Solar Cell," Comsat Technical Review, Vol. 3, No. 1, Spring 1973.
- Raider, S. I. and Berman, A. "On the Nature of Fixed Oxide Charge," J. Electrochemical Society, Vol. 125, No. 4, 1978.
- Revez, A. G. "Anodic Oxidation of Silicon in KNO_3 -N-Methylacetamide Solution: Interface Properties," J. Electrochemical Society, Vol. 114, June 1967.
- Revez, A. G. "Noncrystalline Silicon Dioxide Films on Silicon: A Review," Journal of Non-Crystalline Solids, Vol. 11, 1973.
- Salter, G. C. and Thomas, R. E., "Induced Junction Solar Cells," Conference Record of the 11th Photovoltaic Specialists Conference, 1975.
- Schmidt, E. "Single Method for the Determination of Optical Constants of Absorbing Materials," Applied Optics, Vol. 8, No. 9, 1969.
- Sze, S. M. Physics of Semiconductor Devices, Wiley-Interscience, 1969.
- Tyagai, V. A. "Study of the Nature of a Pulsed Photoeffect at a Cadmium Sulfide Electrolyte Solution Interface," Soviet Physics-Solid State, Vol. 6, No. 6, December, 1964.
- Vasil'ev, V. K., Zorin, E. I., Pavlov, P. V. and Tetel'baum, D. I., "Electrical Properties of Inversion Layers Produced in Silicon by Bombardment with Phosphorus and Aluminum Ions," Soviet Physics-Solid State, Vol. 9, No. 7, January 1968.
- Zaghloul, A. R. M., Azzam, R. M. A. and Bashara, N. M. " SiO_2 -Si Film-Substrate Single-Reflection Retarders for Different Mercury Spectral Line," Optical Engineering, Vol. 17, No. 2, March-April, 1978.